Titanite petrochronology linked to phase equilibrium modelling constrains tectono-thermal events in the Akia Terrane, West Greenland

C.L. Kirkland[a,*], C. Yakymchuk[b], N.J. Gardiner[c], K. Szilas[d], J. Hollis[e], H. Olierook[a], A. Steenfelt[f]

[a] Centre for Exploration Targeting – Curtin Node, The Institute for Geoscience Research, John de Laeter Centre, School of Earth and Planetary Sciences, Curtin University, Perth, Western Australia 6102, Australia
[b] Department of Earth and Environmental Sciences, University of Waterloo, Waterloo, Ontario N2L 3G1, Canada
[c] School of Earth and Environmental Sciences, University of St. Andrews, St. Andrews KT16 9AL, United Kingdom
[d] Department of Geosciences and Natural Resource Management, University of Copenhagen, Øster Voldgade 10, 1350 Copenhagen, Denmark
[e] Geology Department, Ministry of Mineral Resources, Government of Greenland, P.O. Box 930, 3900 Nuuk, Greenland
[f] The Geological Survey of Denmark and Greenland, Copenhagen, Denmark

ARTICLE INFO

ABSTRACT

The Mesoarchean Akia Terrane in West Greenland contains a detailed magmatic and metamorphic mineral growth record from 3.2 Ga to at least c. 2.5 Ga. This time span makes this region an important case study in the quest to track secular changes in geodynamic style which may ultimately inform on the development of plate tectonics as a globally linked system of lateral rigid plate motions. The common accessory mineral titanite has recently become recognised as a powerful high temperature geochronometer whose chemistry may chart the thermal conditions of its growth. Furthermore, titanite offers the potential to record the time-temperature history of mafic lithologies, which may lack zircon. Although titanite suffers from higher levels of common Pb than many other U–Pb chronometers, we show how measurement of $^{207}Pb/^{206}Pb$ in texturally coeval biotite may assist in the characterization of the appropriate common Pb composition in titanite. Titanite extracted from two samples of mafic gneisses from the Akia Terrane both yield U–Pb ages of c. 2.54 Ga. Although coeval, their chemistry implies growth under two distinctly different processes. In one case, the titanite has elevated total REE, high Th/U and grew from an in-situ partial melt, consistent with an identical date to granite dyke zircon. In contrast, the second titanite sample contains greater common Pb, lower total REE, lower Th/U, and grew from dominantly hydrothermal fluids. Zr-in-titanite thermometry for partial melt-derived titanite, with activities constrained by phase equilibrium modelling, indicates maxima of c. 690 °C. Elsewhere in the Akia Terrane, coeval metamorphism linked to growth of hydrothermal titanite is estimated at temperatures of c. 670 °C. These new results when coupled with existing findings indicate punctuated, repeated metamorphic events in the Akia Terrane, in which high temperature conditions (re)occurred at least three times between 3.0 and 2.5 Ga, but crucially changed in style across a c. 3.0 Ga change point. We interpret this change in metamorphism as reflecting a fundamental shift in geodynamic style in West Greenland at 3.0 Ga, consistent with other estimates for the onset of widespread plate tectonic-type processes.

1. Introduction

To effectively document the secular evolution of Earths geodynamic state from the rock record, it is necessary to integrate both pressure–temperature information with accurate temporal constraints. In this regard, titanite has come to be recognised as a high temperature U–Pb chronometer, with a likely Pb diffusion temperature of > 830 °C (Corfu, 1996; Kylander-Clark et al., 2008; Kohn and Corrie, 2011; Hartnady et al., 2019). Further, titanite is a powerful tool to constrain the age of mafic units via U–Pb geochronology in which zircon is often not present (Corfu, 1996; Gao et al., 2012; Garber et al., 2017; Kohn, 2017; Hartnady et al., 2019). Coupled with its use as a geochronometer, the Zr contents of titanite can be used as a geothermometer (Hayden et al., 2008), which permits temperature–time points to be constructed, if the activities of titania and silica during titanite growth can be determined.

Archean West Greenland has been a fundamental study area for the development of concepts related to horizontal (subduction zone) tectonics on the early Earth (Talbot, 1973; Bridgwater et al., 1974; Garde
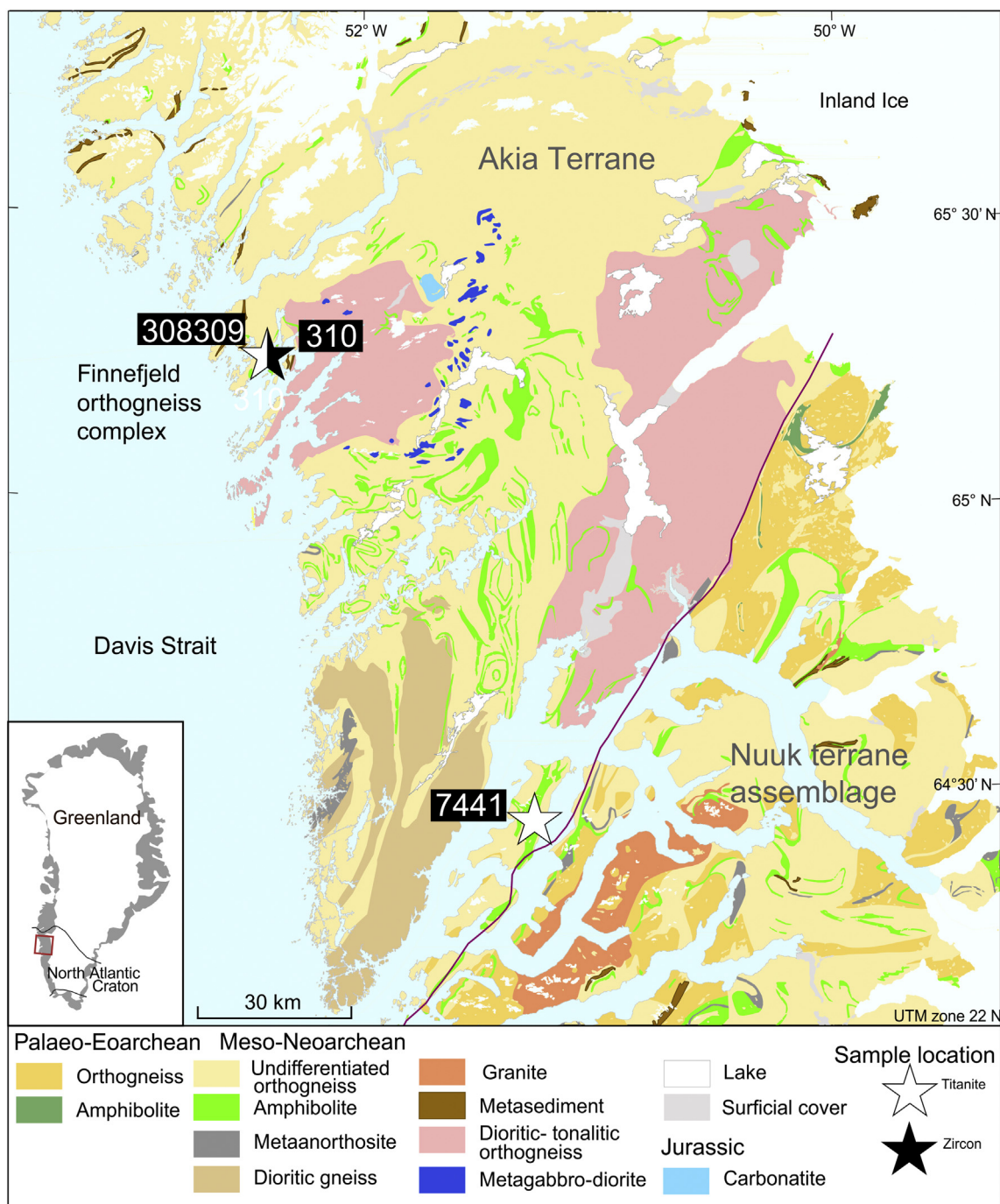
Fig. 1. Map of the Akia and Nuuk terranes of the North Atlantic Craton (modified from Gardiner et al., 2019).

et al., 2000; Garde, 2007; Friend and Nutman, 2005; Kusky et al., 2018; Friend and Nutman, 2019). More globally, the period 3.2–2.5 Ga is a key period in Earth history, both in terms of craton assembly, and also when some researchers argue that many geochemical proxies point to a global shift in tectonic style (e.g. Dhuime et al., 2012; Naeraa et al., 2012). The Akia Terrane of West Greenland (Friend et al., 1988) is a major Mesoarchean terrane, which witnessed crustal growth from 3.2–3.0 Ga and then a complex thermal history from 2.8–2.5 Ga (Garde, 1997; Gardiner et al., 2019; Yakymchuk et al., 2020; Kirkland et al., 2018a). It thus makes an ideal study area in which to investigate changes in magmatism which may be linked to changes in geodynamic style, during this key period in Earth history (Shirey and Richardson, 2011; Cawood et al., 2018; Hartnady and Kirkland, 2019).

In this study we present combined phase equilibrium *P–T* modelling, U−Pb geochronology and trace-element geochemistry of titanite in migmatitic amphibolitic gneisses from the margins of the Mesoarchean crust of the Akia Terrane (Fig. 1). We examine a metavolcanic rock of intermediate composition to further constrain the behaviour of the U−Pb isotope system in titanite during metamorphic/metasomatic processes. We appraise $^{207}Pb/^{206}Pb_c$ (where Pb_c denotes the common Pb component) in both biotite and plagioclase to characterize the common Pb composition for titanite age calculations. This work provides new pressure–temperature–time (*P-T*-t) information that enable us to evaluate the tectonic evolution of the Akia Terrane localities during a potentially critical time in Earth history when modern style subduction may have become the predominant form of crustal growth

and recycling due to the progressive change in planetary thermal state.

1.1. Regional geology

In West Greenland, north of the capital Nuuk, the Akia Terrane (Fig. 1) has been suggested to have developed at 3076–≤3068 Ma in a magmatic arc that accreted to a c. 3200 Ma Paleo- to Mesoarchean core (Garde, 2007; Garde et al., 2012). Voluminous emplacement of Mesoarchean tonalite–trondhjemite–granodiorite (TTG) gneisses and synchronous low-pressure granulite-facies metamorphism and late-tectonic felsic magmatism followed this inferred arc magmatism (Garde et al., 2000).

On the basis of a regional zircon U-Pb-Hf campaign, Gardiner et al. (2019) interpreted that the continental crust that volumetrically dominates the Akia Terrane, and which was formed through two major magmatic phases at c. 3.2 Ga and more significantly at c. 3.0 Ga (Garde et al., 2000; Baadsgaard and McGregor, 1981), may have been derived from partial melting of a mafic precursor, and further that this mafic parent may be Eoarchaean or even older in age. Importantly, no magmatic rocks have been dated in the intervening period between the two major phases of felsic crust production, and no evidence for the involvement of pre-existing felsic crust was found across the region. Following this isotopic evidence, Gardiner et al. (2019) highlighted a potential role for the derivation of the felsic crust through deep infracrustal melting of older, thickened mafic crust, which in some cratons such as the Pilbara, is linked to a vertical tectonic setting (e.g. Johnson et al., 2017; Smithies et al., 2007).

In a radical alternative interpretation, Garde and others (Garde et al., 2012, 2014; Scherstén and Garde, 2013; Keulen et al., 2015) suggested that a giant bolide at ≥3000 Ma, potentially responsible for what these authors interpret as the oldest known extant impact structure on Earth, was the driver for a Mesoarchean thermal event within the Akia Terrane. This event was considered to have resulted in a range of melting and cataclastic features in the region. Elsewhere, bolide impacts have been considered as a viable means of producing felsic crust through melting and then fractional crystallization of an originally homogeneous crust of granodioritic (Latypov et al., 2019) or mafic composition (Johnson et al., 2018).

Metamorphism in the northern Akia Terrane commenced at 2989 ± 5 Ma and was associated with widespread granulite-facies imprint on the rocks (Yakymchuk et al., 2020). These authors reported orthopyroxene-bearing metamorphic assemblages in these rocks consistent with suprasolidus conditions at pressures of < 9 kbar and temperatures > 750 °C, which locally may have exceeded 900 °C across the Akia Terrane during the first widespread metamorphic event affecting the region (Friend and Nutman, 1994; Garde et al., 2000; Riciputi et al., 1990). Late Archean Granulite-facies metamorphism is also known throughout west Greenland and occurred at least twice pre- and also post- dating 3.0 Ga magmatism (Riciputi et al., 1990; Friend and Nutman, 2019).

A second metamorphic event at c. 820–850 °C and 8–10 kbar in the period 2857–2700 Ma is linked to regional deformation (Kirkland et al., 2018a). Some supracrustal rocks within the Akia Terrane were deposited in the period ≤2877 Ma and ≥2857 Ma onto a basement of c. 3.0 Ga tonalites with rare c. 3.2 Ga diorites (Kirkland et al., 2018a). After deposition, these supracrustal rocks were buried to > 30 km depth, where they experienced partial melting. The timing and nature of this late Meso- to Neoarchean metamorphism in the Akia Terrane is broadly consistent with similar conditions in surrounding terranes in West Greenland (Næraa and Scherstén, 2008; Dziggel et al., 2014).

A third metamorphic event at c. 2630 Ma, with loosely constrained conditions somewhere between > 450 to < 850 °C, has been discerned on the basis of Pb diffusion modelling and U–Pb geochronology of metamorphic zircon overgrowths and neoblastic apatite (Kirkland et al., 2018b). This event was coeval with supracrustal-hosted orogenic gold mineralization in the Nuuk region (Nutman et al., 2007), and may

reflect terrane accretion (Nutman and Friend, 2007). Hence, at least three metamorphic episodes are already characterized from the Akia Terrane. Near Nuuk on Store Malene, Nutman et al. (2010) have demonstrated a tectonothermal event continuing to at least 2531 ± 4 Ma, which is proximal to sample 7441. Furthermore, Garde et al. (2000) report 2546 ± 6 Ma amphibolite facies metamorphism on the NW side of the Akia Terrane, near sample 308309. The sequencing, P–T conditions and duration of these discrete metamorphic events may be characteristic of the geodynamic processes operating at that time.

The Akia Terrane has thus experienced a protracted Mesoarchean–Neoarchean magmatic and metamorphic history which straddles a key period in Earth history, a period proposed by some workers to encompass the onset of widespread subduction processes (e.g. Dhuime et al., 2012) perhaps linked to the development of Plate Tectonics on Earth. Thus, we consider that the Akia Terrane is an excellent candidate with which to constrain the P-T-t conditions of crust production, reworking and metamorphism during this key point in Earth history. In this work we review the petrogenesis of titanite bearing samples from both the Northern and Southern fringes of the Akia Terrane.

2. Methods

2.1. U–Pb titanite LA-ICPMS

Titanite U–Pb and trace-element compositions were obtained at the GeoHistory Facility in the John de Laeter Centre, Curtin University in Perth, Australia. Titanite grains were ablated using a Resonetics RESOlution M-50A-LR system incorporating a COMPex 102, 193 nm excimer UV laser. Analyses were performed at a 5 Hz laser repetition rate with a laser fluence of 2.6 J·cm^{-2} as measured on the sample surface. Throughout the ablation the sample cell was flushed with ultrahigh purity He (350 mL·min^{-1}) and N (3.8 mL·min^{-1}). Further details on the titanite analytical protocol are given in Kirkland et al. (2018c). Isotopic abundances were measured using an Agilent 8900 triple quadrupole ICPMS, with high purity Ar as the plasma gas (1 L·min^{-1}). A spot size of 50 μm was used for analyses on individual titanite grains mounted in epoxy resin (sample 308309). A 10 μm spot size was used for titanite analyses on thin section (sample 7441). Ablation times of 30 s bracketed between two 20 s periods of background collection were used. Most trace elements were analysed for 0.01 s, but the dwell time was increased to 0.05 s for ^{204}Pb, ^{206}Pb, ^{207}Pb, ^{208}Pb, ^{232}Th and ^{238}U.

U–Pb LA-ICP-MS data were reduced using VisualAge UComPbine data reduction scheme in Iolite and in-house excel macros (Chew et al., 2014; Paton et al., 2011). The primary age standard used for the titanite analyses was OLT1 (1015 ± 2 Ma; Kennedy et al., 2010). Titanite standard BLR-1 (1047.1 ± 0.4 Ma; Aleinikoff et al., 2007) was run as an unknown and a regression from contemporaneous Stacey and Kramers terrestrial model common Pb through the uncorrected data for BLR-1 yielded a date of 1047 ± 6 Ma (MSWD = 0.63, n = 15). We calculate F207 to assess the amount of common Pb within titanite analyses. F207 is the distance upwards along a mixing line towards common Pb from radiogenic Pb where 100% represents an analysis dominated by the common component. F207 can be readily calculated as the percentage difference between the U/Pb ratio predicted for concordance at the 207-corrected date versus the measured U/Pb ratio.

Trace-element data were reduced using the Trace-element IS data reduction scheme in Iolite (Paton et al., 2010). MKED1 (Spandler et al., 2016) was used as the primary standard to calculate elemental concentrations (using ^{47}Ti as the internal standard element) and to correct for instrument drift. 18.16 wt% Ti was assumed for titanite unknowns. Secondary trace element standards (OLT1, BLR-1, NIST 610, NIST 612) reproduce recommended values to within 2% for all elements when reduced using appropriate matrix matched standard. Titanite U–Pb and trace-element data are present in Supplementary Table 1.

Table 1
Whole-rock compositions used in phase equilibrium modelling.

	Wt%											
Sample	SiO_2	TiO_2	Al_2O3	Fe_2O_3T	CaO	MgO	Na_2O	K_2O	MnO	P_2O_5	LOI	Total
308,309	48.90	0.61	14.40	11.00	12.20	7.89	1.79	0.26	0.19	0.04	1.05	98.33
7441	60.41	0.65	16.00	5.25	8.79	2.19	2.89	1.14	0.16	0.18	2.86	100.52
	Mol.%											
Sample	Figure	H_2O	SiO_2	Al_2O_3	CaO	MgO	FeO	K_2O	Na_2O	TiO_2	O	Total
308,309	7	4.06	50.30	8.73	13.44	12.01	8.51	0.17	1.78	0.47	0.43	100.00
7441	8	1.71	65.48	10.22	10.21	3.54	4.28	0.79	3.03	0.53	0.22	100.00

Fe_2O_3T = Total Fe as Fe_2O_3

2.2. Pb−Pb plagioclase and biotite LA-ICPMS

Biotite and plagioclase were also analysed in thin section on sample 7441 by LA-ICPMS (using the same analytical equipment as titanite). External standardization is required in LA-ICPMS analysis to correct for time-dependent elemental fractionation during ablation and instrumental drift over the course of an analytical session. It is widely recognised that variable laser-target interactions can lead to sample/standard matrix mismatches that cause cryptic biases in externally calibrated U−Pb ages. Nonetheless, in the case of plagioclase and biotite where U content can be demonstrated to be low to below detection and hence where the $^{207}Pb/^{206}Pb$ ratio reflects a common Pb ratio that is of primary interest (that is, isotopes of the same element), low fractionation analytical settings can be utilized that minimize elemental fractionation to facilitate non-matrix-matched calibration using National Institute of Standards and Technology (NIST) glasses (Horn and von Blanckenburg, 2007). We utilize the analytical procedure discussed in McFarlane (2016) with large (100 μm) and shallow (30 s ablation) pits. Under these conditions no laser-induced fractionation of $^{207}Pb/^{206}Pb$ in NIST 612 or NIST 610 can be discerned and no correction is deemed necessary for this ratio. Hence, no downhole correction is made; instead the mean of each background-corrected 30 s ablation (excluding the first 2 s of data) is used. Normalisation of the U/Pb ratio is based on the measured/accepted ratio derived from the session-based drift-corrected mean of the NIST 610 reference material. Working values of $^{206}Pb/^{238}U$ (0.2236 ± 0.015) are taken from Horn and von Blanckenburg (2007) and a U/Pb fractionation correction factor is derived using this value. Biotite and plagioclase U−Pb data are given in Supplementary Table 2.

2.3. U−Pb zircon SHRIMP

U−Pb geochronology of zircon crystals from sample 310 were conducted on SHRIMP-B in the John de Laeter Centre at Curtin University, Perth Australia. Nineteen analyses of standard material 91500 were obtained throughout the session yielding a spot-to-spot uncertainty of 0.5% (1σ) and a $^{238}U/^{206}Pb$ calibration uncertainty of 1.3% (1σ). Both internal and external errors were propagated in quadrature. Twenty-eight analyses of zircon standard Plešovice (Sláma et al., 2008; 337.13 ± 0.37) were also conducted to verify results and yielded a weighted mean $^{238}U/^{206}Pb*$ date of 339 ± 2 (MSWD = 1.2). Common Pb corrections were applied to all analyses using contemporaneous common Pb based on the Pb evolution model of Stacey and Kramers (1975) and the measured ^{204}Pb. Zircon geochronology data are provided in Supplementary Table 3.

2.4. Phase equilibrium modelling

Phase equilibrium modelling allows the calculation of stable phase assemblages as a function of *P* and *T*, for a particular bulk rock composition. Metamorphic assemblages were modelled in the Na_2O–CaO–K_2O–FeO–MgO–Al_2O_3–SiO_2–H_2O–TiO_2–O (NCKFMASHTO) chemical system using activity–composition (a-X) models from Green et al. (2016), the internally consistent thermodynamic database (ds63)

of Holland and Powell (2011), and the THERMOCALC software package (Powell and Holland, 1988). Phases modelled as pure end-members are quartz, titanite, and aqueous fluid (H_2O). Mineral abbreviations are from Holland and Powell (2011), except for titanite (ttn). Modelled samples were assumed to have 10% Fe in the ferric state (Fe^{3+}), as the proportion of ferric to ferrous iron is not expected to have a significant influence on stability field of titanite in metabasite compositions (e.g. Palin et al., 2016). The amount of H_2O in the bulk composition was modified from the LOI value so that the solidus was just saturated with H_2O at 6 kbar (i.e. no free H_2O) at an assumed pressure of 6 kbar. If the prograde *P–T* path crossed the wet solidus at lower or higher *P*, the amount of melt predicted will be slightly overestimated and underestimated, respectively, at suprasolidus conditions. Slight adjustments to the amount of H_2O in the system will change the temperature of the solidus, but the general topology of the diagrams is not expected to change.

The measured and modelled compositions for both samples are shown in Table 1. Activities of titania and silica were calculated using the chemical potentials of TiO_2 and SiO_2 from the 'caclmu' script in THERMOCALC. A grid of points with 1 kbar and 50 °C spacing was used and the results were contoured using Matlab and linear extrapolation between points. Modelled concentrations of Zr in titanite were calculated using expression of Hayden et al. (2008) that considers temperature, pressure and the activities of silica and titania. Modest variations in the amount of H_2O in the modelled compositions are not expected to change a_{SiO2} as the systems are quartz present over most of the modelled *P–T* range. Reduction of the amount of H_2O in the modelled bulk composition will have a small effect on modelled a_{TiO2} due to the reduced stability fields of titanium-bearing hydrous minerals (e.g. amphibole, biotite), but this only slightly affects the estimated concentration of Zr in titanite.

3. Results

All age uncertainties, unless specifically stated otherwise, are given at the 95% confidence level.

3.1. Petrography and field relationships

3.1.1. Sample 308309

Sample 308309 is a foliated migmatitic amphibolite gneiss that is refolded in decimetre scale isoclinal folds (Fig. 2; decimal degrees 65.2433,–52.370278). The gneiss has nebulitic, stromatic, veined and agmatitic textures defined principally by plagioclase and amphibole (kaersutite) dominant layers. Some patches of the rock are leucosome poor, with a broadly chondritic whole rock REE composition for those parts. The rock contains minor quartz, relic clinopyroxene (diopside) and accessory titanite, calcite, wollastonite, apatite, zircon, and ilmenite. Very minor ankerite and sericite are late replacement products. Patchy quartz-feldspar leucosomes contain orthopyroxene and clinopyroxene and are folded. A late generation of tourmaline-bearing felsic dykes (granitic) that do not contain pyroxene cuts the foliation within the rock. Melanocratic layers within the sequence contain
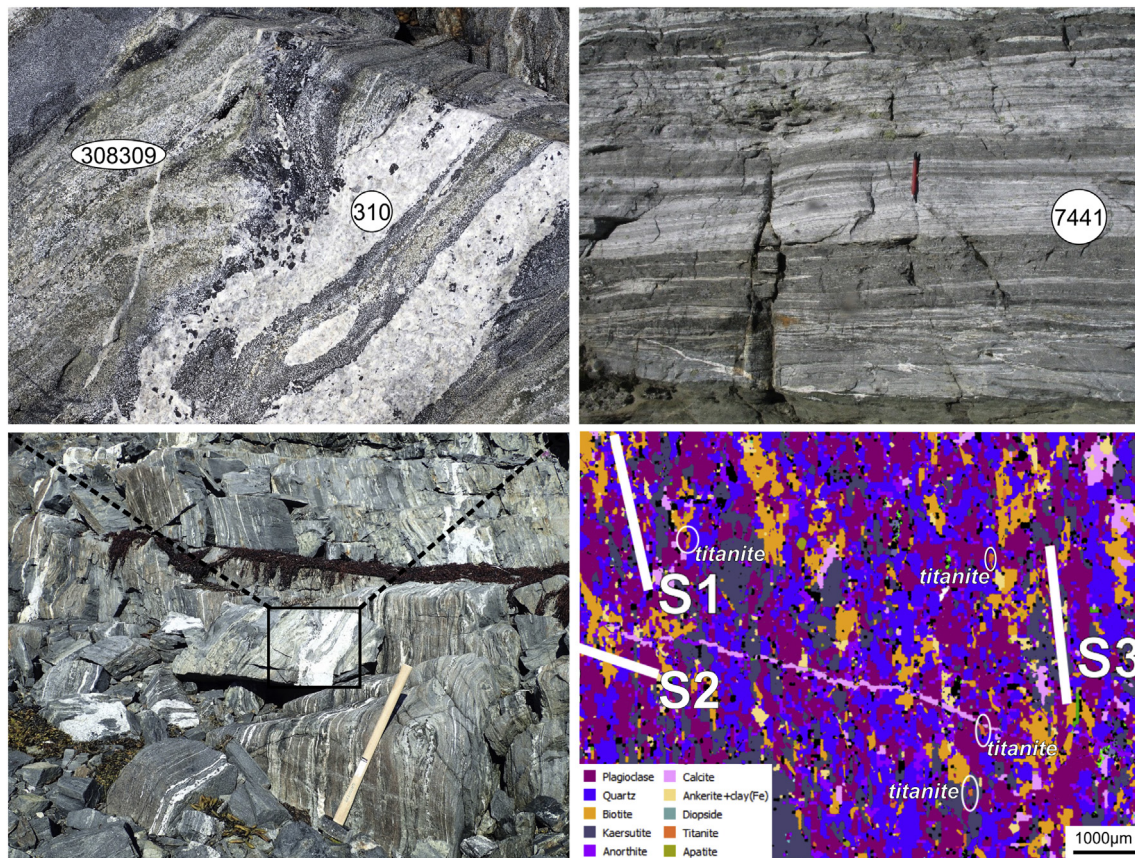
Fig. 2. Left, top and bottom, field photographs of 310 and 308309 sample sites in agmatitic amphibolitic gneiss, Akia Terrane. Right top; field photograph of sample site 7441, leucocratic amphibolite in layered metavolcanic sequence, Akia Terrane. Lower right; automated mineral analysis (TIMA) image coloured for mineral phase highlighting titanite (circled regions) developed along with biotite in a late fabric that cuts calcite veins in sample 7441.

garnet. The geochronology sample for titanite specifically targeted a leucosome rich portion of the rock.

3.1.2. Sample 310

Sample 310 was taken from one of the late generations of granite dyke containing tourmaline that cuts the gneissic foliation (Fig. 2; decimal degrees 64.42146,–51.257129). The dyke is coarse-grained and anastomoses through the gneiss and ponds into 50 cm lozenges.

3.1.3. Sample 7441

This sample is a leucocratic amphibolite (metaandesite) from a layered metavolcanic sequence (Fig. 2) in the Bjørneøen supracrustal belt in the southeastern part of the Akia Terrane. This sequence is part of the Qussuk Supracrustal Belt, for which U−Pb zircon dating has previously yielded an age of 3071 ± 1 Ma from a volcano-sedimentary schist, interpreted as a protolith age (Garde, 2007). The Bjørneøen-Qussuk metavolcanic sequence comprises intercalated tholeiitic meta-basalts (amphibolites) and metaandesites (leucoamphibolites) (Szilas et al., 2017). Sample 7441 is strongly-foliated (Fig. 2) and dominated by amphibole, plagioclase, and quartz. Compositional banding on the 5 mm scale is defined by quartz and plagioclase dominant layers alternating with amphibole (kaersutite) and plagioclase dominate layers. Locally there is diopside associated with calc-silicate boudins, and biotite is present in fractures and as a late foliation parallel phase. Accessory minerals include titanite, apatite, zircon, and calcite. An early amphibole defined foliation is cut at 45° by thin calcite veins, which are themselves cut by a late fabric defined by biotite and titanite that is near-parallel to S0/S1 (Fig. 2). Titanite typically has grain contacts with plagioclase, quartz, and biotite.

3.2. U−Pb geochronology

3.2.1. Sample 308309: titanite

This sample yielded a large proportion of euhedral titanite crystals that range up to 300 μm in length and are remarkably homogeneous in BSE images (Fig. 3). Inclusions in titanite include calcite, ilmenite, perovskite and quartz. U−Pb analysis of this titanite shows a strong correlation between $^{207}Pb/^{206}Pb$ date and U content, where low U content (less than c. 3 ppm) is associated with elevated $^{207}Pb/^{206}Pb$ date. At > 7 ppm U, $^{207}Pb/^{206}Pb$, ages stabilise at c. 2550 Ma. Such relationship is consistent with the greater influence of common Pb, and hence spuriously old $^{207}Pb/^{206}Pb$ ages, in those analyses with low U and thus a low production of radiogenic Pb.

Given the generally low apparent common Pb content in this sample as implied by the U−Pb systematics we use Stacey and Kramers (1975) common Pb for the $^{207}Pb/^{206}Pb$ date of the sample to calculate F207%. Fourteen analyses have > 6% common Pb as estimated by F207 and a further four analyses are on cracks, grain edges, or ablated inclusions; all these analyses are interpreted to have isotopic ratios influenced by common Pb (Group D). In order to further evaluate the Pb isotope systematics of this sample we plot $^{207}Pb/^{206}Pb$ date (Y-axis) versus 207-corrected $^{238}U/^{206}Pb$ date (X-axis) (Fig. 4). On this correlation plot, concordant analyses, with low estimated common Pb, will plot on a 1:1 line whereas analyses with elevated common Pb will plot at higher $^{207}Pb/^{206}Pb$ date for any given 207-corrected date. Conversely, recent radiogenic-Pb loss will cause data to spread to the right on an inverse Concordia diagram, which will affect 207-corrected dates but will not affect $^{207}Pb/^{206}Pb$ dates. Hence, on our age correlation plot, recent radiogenic-Pb loss moves data towards the left. Ancient radiogenic Pb loss will cause a spread in data. In contrast, common Pb contamination,
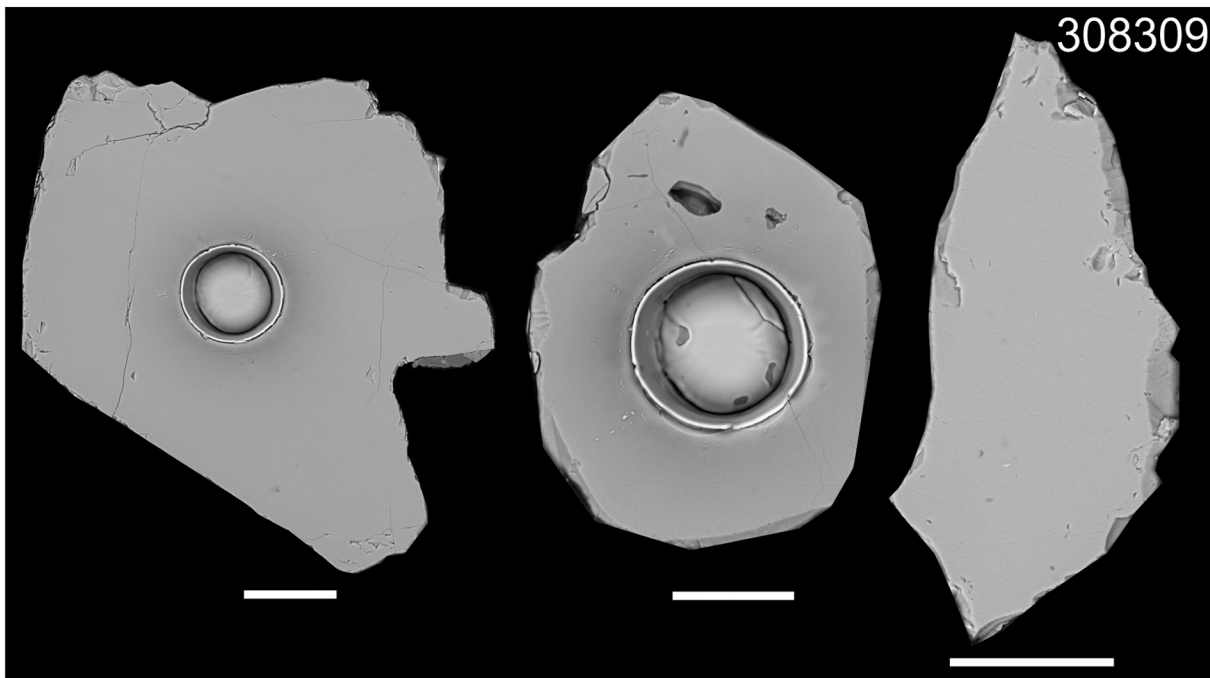
Fig. 3. Backscatter electron image of representative titanite grains from sample 308309 migmatitic amphibolitic gneiss, Akia Terrane, Greenland. Scale bars are 50 μm. Two grains show laser ablation craters.

which drives data upwards and left, towards the common Pb intercept, on an inverse concordia plot, will affect ^{207}Pb/^{206}Pb dates but not alter the ^{207}Pb corrected date, and move data upwards on the correlation plot, if the common Pb composition is constant throughout the sample. Hence, by using the minimum difference between the ^{207}Pb corrected ages and ^{207}Pb/^{206}Pb ages, we highlight analyses with the least common lead content and also least radiogenic-Pb loss. On this plot we also show contours for discordance between ^{207}Pb/^{206}Pb date and 207-corrected date. A conversion of this discordance metric to F207 as a measure of the amount of common Pb modelled on 2500 Ma Stacey and Kramers (1975) common Pb is also given (Fig. 4). Eighty analyses yield 207-corrected dates of 2642–2211 Ma, with a geologically meaningless weighted mean of 2479 ± 23 Ma (MSWD = 5.3). The elevated MSWD indicates that this is not a single population and that there are in all likelihood geological reasons for the scatter in the dataset. The data has a tail to younger dates (both 207-corrected and ^{207}Pb/^{206}Pb), consistent with minor ancient radiogenic Pb loss. Eight near concordant distinctly younger analyses (Group P) yield ^{207}Pb/^{206}Pb dates of 2459–2370 Ma. The analyses do not define a single weighted mean date and no clear correlation is observed between uranium content and date for Group P. Hence, these eight analyses may reflect minor degrees of ancient partial radiogenic Pb loss, perhaps facilitated by fast diffusion pathways. Of the remaining 72 concordant analyses (Group M) a statistically coherent group of 69 yields a weighted mean ^{207}Pb/^{206}Pb date of 2536 ± 7 Ma (MSWD = 2.5), interpreted as the best estimate of the age for radiogenic-Pb retention in this titanite. This age is within uncertainty of a U/ Pb zircon date reported by Garde et al. (2000) for a nearby locality.

3.2.2. Sample 310: zircon

The zircon crystals are subhedral to euhedral, with moderate to high length to width ratios. In CL images, all grains have little to no CL response (Fig. 5) consistent with the high to very high U content in these zircons (344–918 ppm). The analyses are slightly reversely discordant (though within analytical uncertainty of Concordia) likely as a function of a different sputtering response to the lower U standard, nonetheless, using the ^{207}Pb/^{206}Pb ratio ameliorates this effect and also benefits from high count rates (Kirkland et al., 2008). All five analyses (Group I) yield a weighted mean ^{207}Pb/^{206}Pb date of 2537 ± 11 Ma

(MSWD = 1.8), interpreted as the age of leucosome crystallization (Fig. 5).

3.2.3. Sample 7441: titanite, plagioclase and biotite

Titanite, plagioclase and biotite from sample 7441 were analysed in thin section by LA–ICP–MS. Titanite analyses scatter along and off any single common – radiogenic Pb mixing line (Fig. 4). The data does not well-define a mixing line nor does it fall on the concordia curve rendering any calculated ages subject to interpretations on the nature of the common Pb composition. Hence, in order to calculate meaningful ages for this titanite the ^{207}Pb/^{206}Pb ratio of common Pb appropriate for this mineral must be independently determined. Plagioclase contains essentially no U so its ^{207}Pb/^{206}Pb could be a valid estimate for the common Pb component incorporated into the titanite if it grew from a compositionally identical source. Twenty analyses of plagioclase surrounding titanite in the thin section yield a weighted mean ^{207}Pb/^{206}Pb of 1.1011 ± 0.0024 (MSWD = 2.1), comparable to 2950 Ma Stacey and Kramers common Pb estimate (Fig. 4). Using a ^{207}Pb/^{206}Pb$_c$ from this plagioclase indicates a range of apparent 207-corrected ages from 2561 to 1963 Ma, consistent with the growth of titanite at c. 2560 Ma, followed by subsequent Pb loss.

Titanite is present as foliation-parallel grains that range in size from < 100 μm, dominantly inclusion free grains to large > 500 μm poikiloblastic grains with perovskite, biotite, feldspar, apatite, quartz, and calcite inclusions (Fig. 2). Plagioclase in a S0/S1 fabric is cut by S2 calcite veins which in turn are cross cut by a S1 parallel S3 fabric defined by biotite and titanite (Fig. 2). Hence, on these textural grounds plagioclase can be demonstrated to have grown earlier than titanite. Thus, biotite could be a better means of tracking appropriate common Pb for the titanite, if the biotite does not contain appreciable radiogenic ingrowth from U. U−Pb analyses of biotite can be considered as defining two groups (A and B), a cluster with no appreciable U with U−Pb near zero (A) and a second group that lies towards higher U/Pb at lower ^{207}Pb/^{206}Pb (B). All biotite data scatter around a line with an imprecise but, nonetheless, Archean lower intercept. Those analyses in group B show variation in the time resolve ablation signal of U and Th, in contrast to group A whose U signal is near background (Fig. 6). The spikes in U content in group B are consistent with ablation of micro
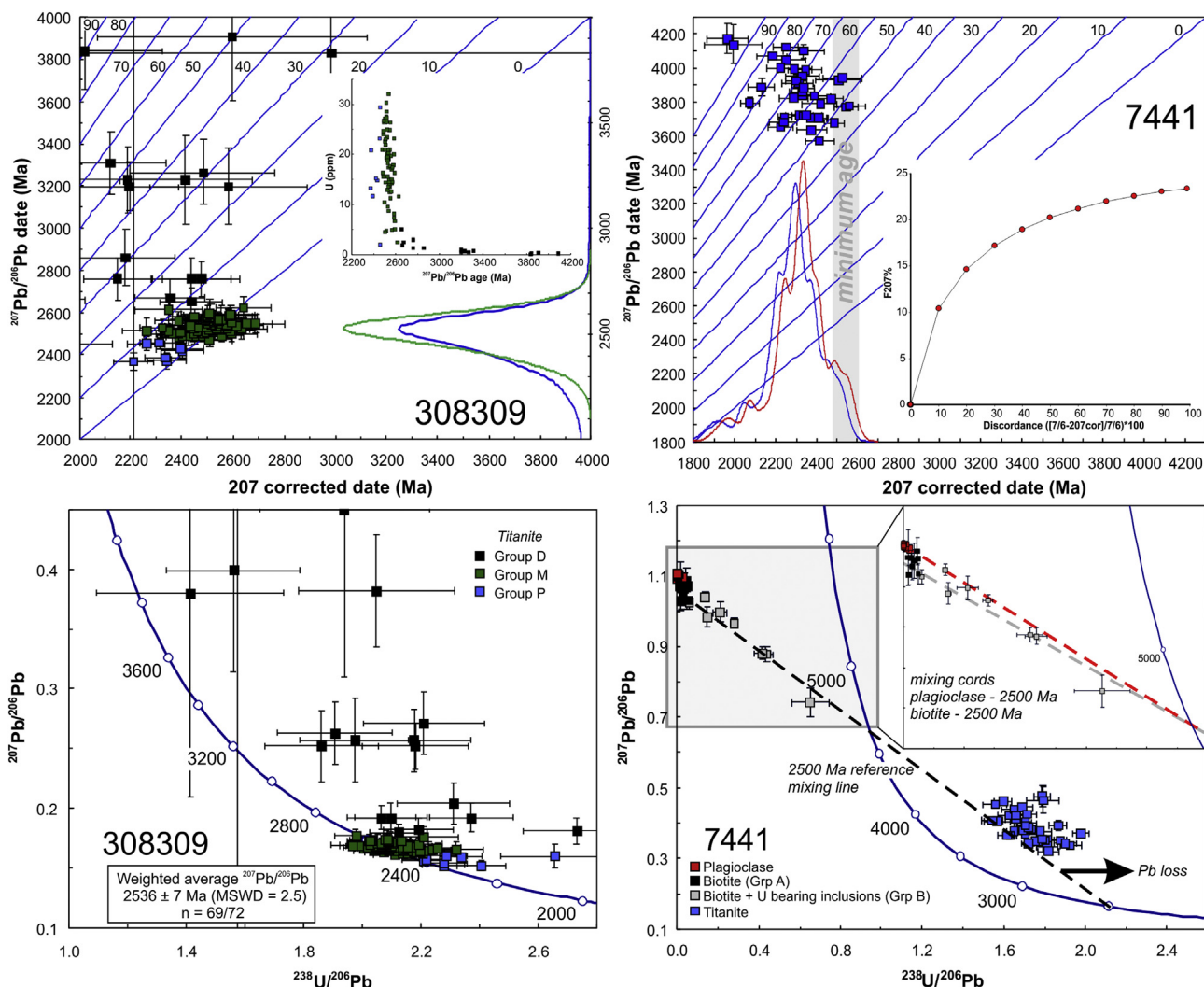
Fig. 4. Top left, ^{207}Pb/^{206}Pb date versus 207-corrected date correlation plot for sample 308309. Inclined lines are discordance as measured as percentage difference of the Pb−Pb versus 207-corrected ages. Probability density curves are for ^{207}Pb/^{206}Pb ages; green curve = Group M, blue curve = all data. Inset: plot of U concentration versus ^{207}Pb/^{206}Pb date. Top right, ^{207}Pb/^{206}Pb date versus 207-corrected date correlation plot for sample 7441. Probability density curves are for 207-corrected ages; red curve = plagioclase based ^{207}Pb/^{206}Pb$_C$, blue curve = biotite based ^{207}Pb/^{206}Pb$_C$. Inset: plot of discordance (between Pb−Pb and 207-corrected ages) versus F207 as modelled from 2500 Ma Stacey and Kramers (1975) common Pb. Lower left, inverse Concordia plot for titanite from sample 308,309, error bars are at the two sigma level. Lower right, inverse Concordia plot for titanite, plagioclase, and biotite from sample 7441, reference radiogenic-common Pb mixing lines are shown. Inset is enlargement of ordinate intercept. (For interpretation of the references to colour in this figure legend, the reader is referred to the web version of this article.)

inclusions of zircon or monazite in the biotite. Therefore, we consider the weighted mean of group A biotite of 1.059 ± 0.017 (MSWD = 2.4), equivalent to a 2540 Ma Stacey and Kramers common Pb estimate, to best reflect the common Pb composition incorporated into titanite. Using this common Pb value yields apparent 207-corrected dates ranging from 2527 to 1915 Ma. The oldest analysis using this correction approach yields a date of 2527 ± 38 Ma (1σ), which we interpret as the minimum age of radiogenic Pb retention in this titanite. Given the distribution of data, recent radiogenic-Pb loss is feasible to explain much of the off-mixing cord scatter in this dataset (Fig. 4).

3.3. Phase equilibrium modelling

3.3.1. Sample 308309

The calculated phase assemblages as a function of *P* and *T* for sample 308309 are shown in Fig. 7a, based on the whole rock composition from a leucosome free portion of this rock. Similar to most metabasites, the wet solidus occurs at ~700 °C with an assemblage of hornblende, plagioclase, clinopyroxene and quartz with titanite at >

5.5 kbar, and ilmenite and biotite without titanite at < 5.5 kbar. The upper temperature limit of titanite stability varies from ~750 °C at > 5 kbar to < 700 °C at 3 kbar. Titanite and anatectic melt are predicted to be stable at > 4 kbar and > 700 °C across the modelled *P*–*T* range. At higher temperatures, hornblende breakdown to orthopyroxene is predicted at > 800 °C and quartz is exhausted by 800 to 900 °C with increasing pressure. Rutile is absent from the modelled assemblage over the investigated *P*–*T* range.

The activities of titanium dioxide, here referred to as (TiO$_2$) titania, (Fig. 7b) and silica (Fig. 7c) vary as a function of pressure and temperature (Ghiorso and Gualda, 2013). Modelled titania activities (relative to rutile) are 0.50–0.95 over the investigated *P*–*T* range and range from ~0.75 to 0.80 in the stability field of titanite (Fig. 7b). Silica activities (relative to quartz) decrease with increasing temperature above the stability field of quartz. Silica activities in the stability field of titanite are estimated to be 1.0 due to the presence of quartz.

Calculated concentrations of Zr in titanite using the formulation of Hayden et al. (2008) vary from < 10 ppm at low temperatures (< 600 °C) to > 10,000 ppm at ultra-high temperatures (900 °C)
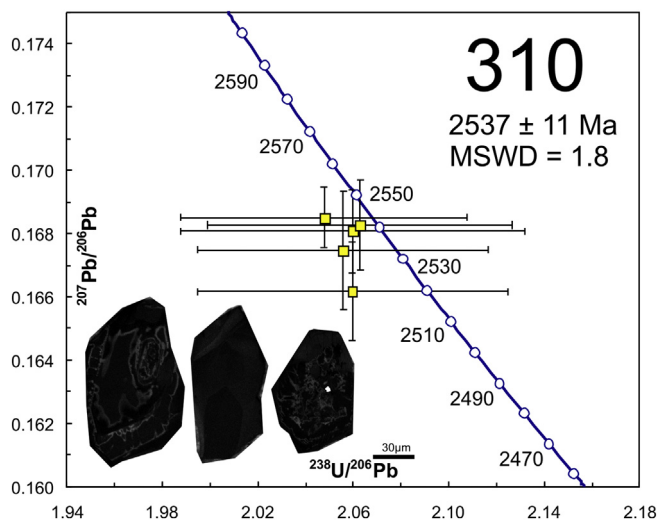
Fig. 5. Inverse Concordia plot for zircon from sample 310. Error bars are at the two-sigma level. Inset: cathodoluminescence images of representative zircon grains.
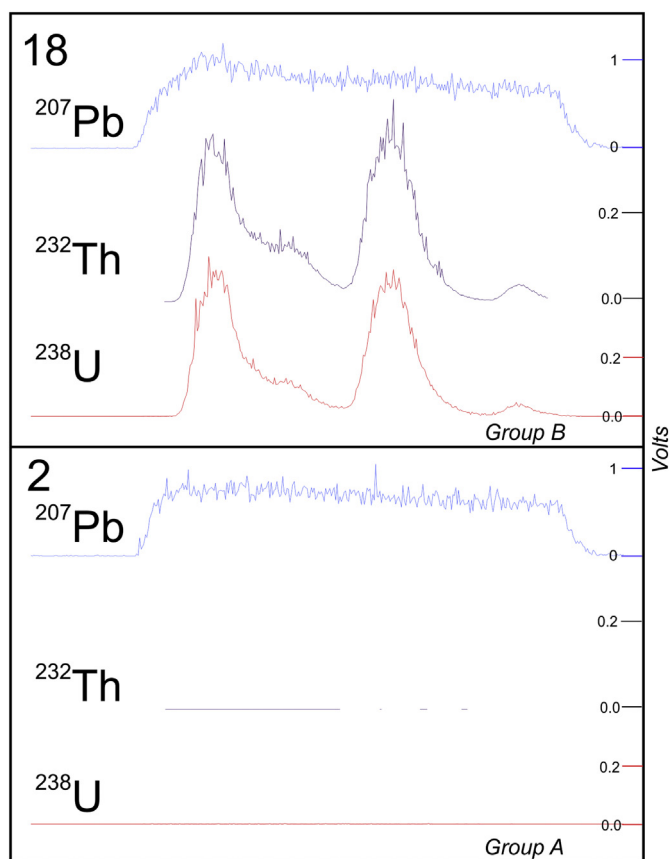

Fig. 6. Ablation time voltage signal for spots 18 and 2 in 7441 biotite. Spot 18 is interpreted to have ablated inclusions of monazite or zircon on the basis of spikes in Th and U channels, in contrast spot 2 signal shows no evidence for inclusions within the biotite.

(Fig. 7d). Modelled concentrations of Zr in titanite in the predicted stability field of titanite extend to ~400 ppm at ~750 °C. The average concentration of Zr in Group M titanite from sample 308309 (~290 ppm; Supplementary Table 1) corresponds to temperatures of 700–750 °C with increasing pressure (Fig. 7e); this value intersects the modelled stability field of titanite at < 6 kbar for sample 308309

(Fig. 7e). The maximum measured concentration Zr in Group M titanite (~470 ppm; Supplementary Table 1) yields temperatures of ~750 °C that are slightly higher than the modelled stability field of titanite for sample 308,309 (Fig. 7e). The minimum value of Zr in Group M titanite (~120 ppm; Supplementary Table 1) is restricted to 650–700 °C, over the modelled *P–T* range. In general, the measured concentrations of Zr in titanite are compatible with temperatures in the suprasolidus titanite stability field at > 700 °C, although the highest observed concentrations are predicted at temperatures just above the inferred maximum stability of titanite.
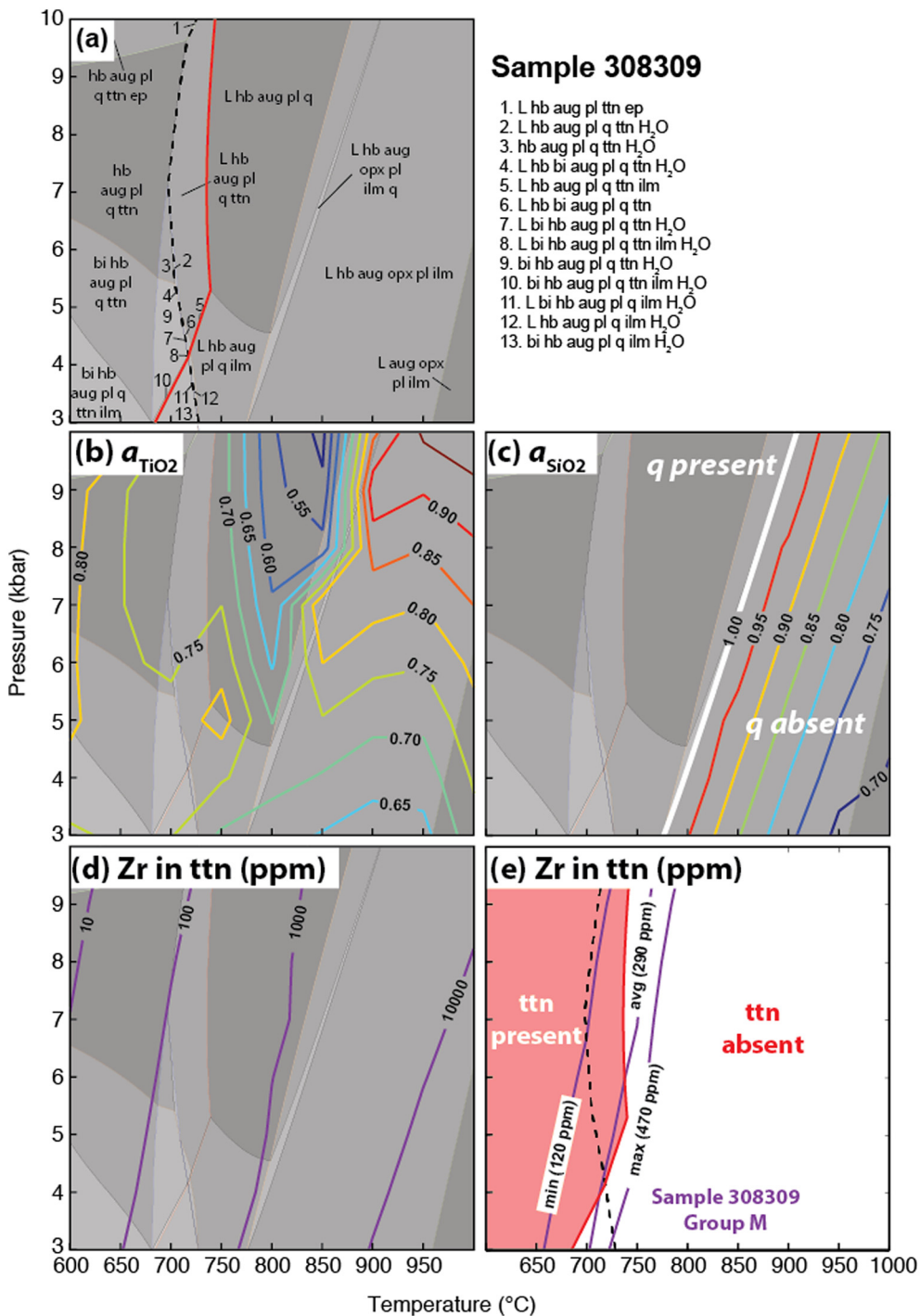
3.3.2. Sample 7441

A pseudosection for sample 7441 showing calculated stable phase assemblages is shown in Fig. 8a. The assemblages are similar to those in sample 308309 with the following exceptions. (i), garnet is predicted to be stable at > 8 kbar in sample 7441, whereas garnet is not predicted to be stable over the modelled P–T range for sample 308309. (ii), titanite is estimated to be stable up to 800 °C at high P whereas in sample 308,309 titanite is predicted to be stable at < 750 °C. (iii), rutile is predicted to be stable at > 950 °C and > 8 kbar. (iv), quartz is stable across the entire modelled P–T range for sample 7441 except at > 950 °C and < 4 kbar (Fig. 8a). Titanite and anatectic melt are stable together at > 650–700 °C, over the modelled pressure range.

Predicted titania activities (relative to rutile) vary from 0.6 to 1.0 across the modelled P–T range and range from 0.70 to 0.95 in the stability field of titanite (Fig. 8b). Silica activities (relative to quartz) are 1.0 except for the small field where quartz is absent at > 950 °C and < 4 kbar, where silica activities are slightly < 1.0.

Using the modelled titania and silica activities, calculated concentrations of Zr in titanite vary from < 10 ppm at high P and low T to > 10,000 at ultrahigh-temperature (> 900 °C) conditions. In the stability field of titanite, modelled concentrations of Zr in titanite range from < 10 to ~200 ppm. The maximum concentration of Zr in titanite (~750 ppm) plots ~50 °C above the maximum calculated stability of titanite whereas the average value (~290 ppm) plots roughly along the titanite-out field boundaries (Fig. 8e). The minimum measured concentration of Zr in titanite is consistent with temperatures of > 650–700 °C with increasing pressure. With the exception of < 5 kbar, all the measured values of Zr in titanite plot above the calculated wet solidus for sample 7441 (Fig. 8).

3.4. Titanite geochemistry

Titanite is an important factor controlling the rare earth element (REE) distribution in a wide variety of rock compositions and geochemical processes because it is one of the most common and pervasive accessory phases, and it has the ability to incorporate large quantities of the light REE (LREE) in its crystal structure (Henderson, 1980). The REE content of titanite helps to interpret both the U−Pb geochronology and Zr-in titanite thermometry (Olierook et al., 2019). Diffusive re-homogenization of titanite trace-element patterns on geologically realistic time scales is unlikely to occur at temperatures below c. 800 °C (Cherniak, 1995); these temperatures are required for titanite to be stable in the investigated samples (Figs. 7, 8). Except in a case of re-homogenization by dissolution–reprecipitation processes, titanite will probably dominantly record the original fluid trace-element chemistry from the time of mineral growth. Comparison between the effective ionic radius of Ca^{2+} and the trivalent REE in seven-fold coordination from thermodynamic models for titanite–melt fractionation (Tiepolo et al., 2002; Prowatke and Klemme, 2005) shows the closest correspondence in radii between Ca and Sm, Eu and Gd. Hence, on the basis of accommodation into the titanite lattice this would suggest that, in the absence of fluid speciation control, titanite–aqueous fluid partitioning should lead to preferential incorporation of the middle REE (MREE) into titanite (e.g. Smith et al., 2009).

Fig. 7. Results of phase equilibrium modelling of sample 308309. (a) Predicted phase assemblages. The red line is the upper temperature limit of titanite stability. The thick dashed line is the solidus. (b) Titania activities (relative to rutile) as a function of pressure and temperature. (c) Silica activities (relative to quartz) as a function of pressure and temperature. All fields to the left (lower T) of the thick white line are predicted to have silica activities of 1.0. (d) Calculated concentration of Zr in titanite (using the model of Hayden et al., 2008) over the modelled P–T range. (e) Contours representing the P–T conditions reflected by the measured concentrations of Zr in titanite in sample 308309 from the Group M population. (For interpretation of the references to colour in this figure legend, the reader is referred to the web version of this article.)

3.4.1. Sample 308309

In sample 308309 evidence for dissolution–reprecipitation processes are not observed in any of the titanite since, under BSE imaging, these grains have a homogeneous response. Titanite grains from sample 308309 (excluding Groups D and P) are enriched in total REE relative to the bulk rock and especially enhanced in LREE (Fig. 9). The REE pattern is consistent with fluid mediated enrichment (enhanced LREE) during partial melting of a broadly basaltic composition (e.g. Storey et al., 2007). The whole rock composition reflects that of a leucosome free portion of the rock. The relatively high Th/U ratios and high Zr and Nb concentrations in the titanite also argue for a silicate-based fluid (e.g. melt) origin for the grains (Olierook et al., 2019), as these elements are generally considered to be broadly immobile in aqueous (i.e.

hydrothermal) fluids. On these grounds we interpret Group M titanite in sample 308309 to reflect high-grade metamorphism, synchronous melting, and injection of ex-situ felsic veins. The titanite ages are consistent with the date of a cross-cutting granite (as measured in zircon; sample 310). The results of the phase equilibrium modelling coupled with Zr-in-titanite thermometry are also consistent with minor degrees of partial melting within the stability field of titanite (Fig. 7). Titanite analyses in Group D have low U, correspondingly low radiogenic Pb, and are characteristically depleted in total REE content. Given the realisation that the U−Pb systematics of titanite can be robust even during high-temperature metamorphism (Corfu, 1996; Walters and Kohn, 2017; Hartnady et al., 2019), it is reasonable to consider the potential that the coherent 3.2 Ga ([207]Pb/[206]Pb date) component in
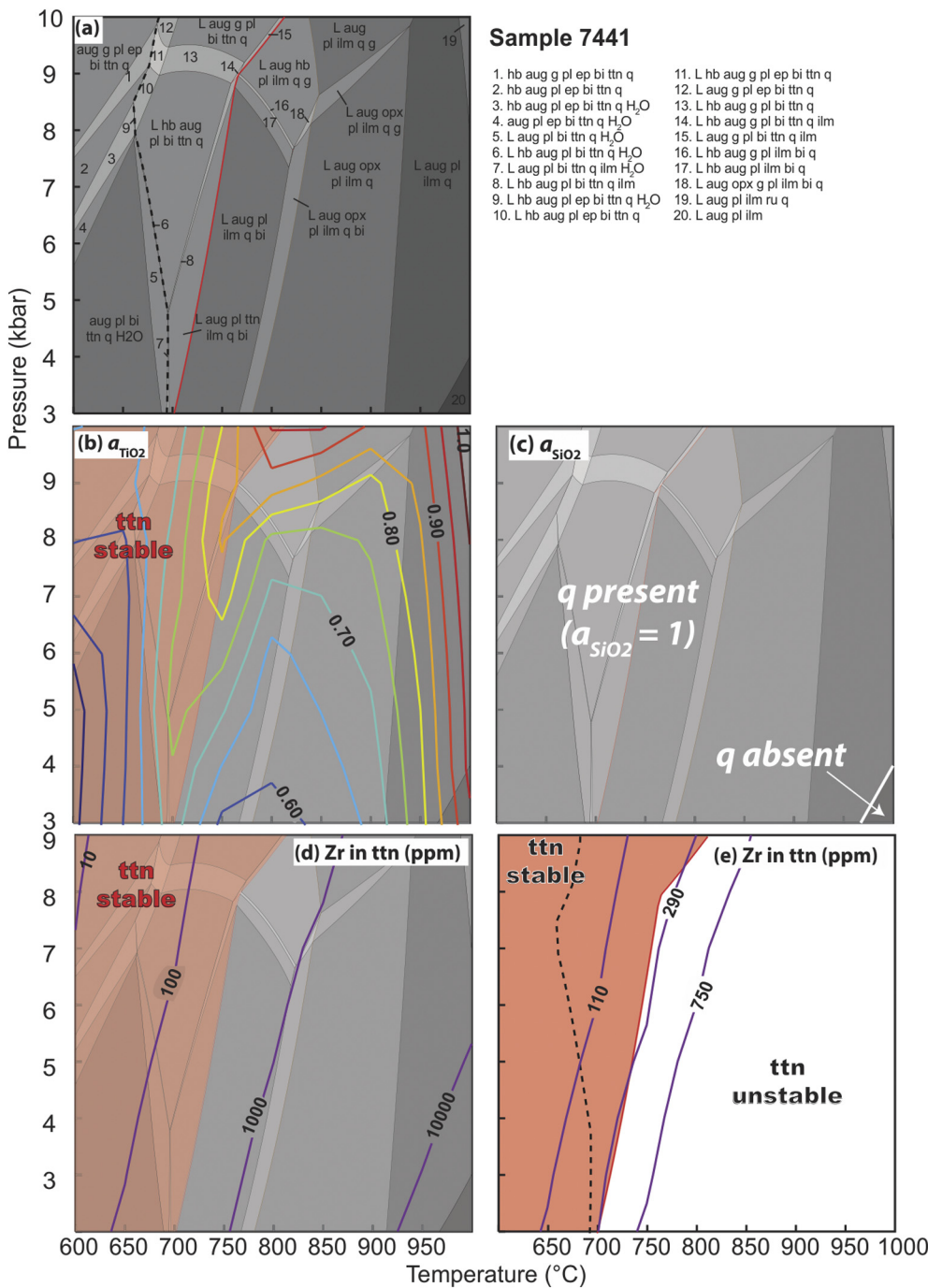
Fig. 8. Results of phase equilibrium modelling of sample 7441. (a) Predicted phase assemblages. The red line is the upper temperature limit of titanite stability. The thick dashed line is the solidus. Quartz is predicted to be stable over the entire modelled P–T range except for the small field at > 950 °C and < 4 kbar. (b) Titania activities (relative to rutile) as a function of pressure and temperature. (c) Silica activities relative to quartz are estimated to be 1.0 except for this small field at high temperature and low pressure. (d) Calculated concentration of Zr in titanite (using the model of Hayden et al., 2008) over the modelled P–T range. (e) Calculated concentration of Zr in titanite for the measured minimum (110 ppm), average (290 ppm) and maximum (750 ppm) concentrations of Zr in titanite from sample 7441. (For interpretation of the references to colour in this figure legend, the reader is referred to the web version of this article.)

Figure content (Sample 7441):

1. hb aug g pl ep bi ttn q
2. hb aug pl ep bi ttn q
3. hb aug pl ep bi ttn q H_2O
4. aug pl ep bi ttn q H_2O
5. L aug pl bi ttn q H_2O
6. L hb aug pl bi ttn q H_2O
7. L aug pl bi ttn q ilm H_2O
8. L hb aug pl bi ttn q ilm
9. L hb aug pl ep bi ttn q H_2O
10. L hb aug pl ep bi ttn q
11. L hb aug g pl ep bi ttn q
12. L aug g pl ep bi ttn q
13. L hb aug g pl bi ttn q
14. L hb aug g pl bi ttn q ilm
15. L aug g pl bi ttn q ilm
16. L hb aug g pl ilm bi q
17. L hb aug pl ilm bi q
18. L aug opx g pl ilm bi q
19. L aug pl ilm ru q
20. L aug pl ilm

Group D is protolith or otherwise inherited grains/grain domains. However, no core regions are clearly discerned on backscatter images nor are these Group D grains dissimilar in terms of grain morphology to the other groups. Furthermore, given the scatter in the 3.2 Ga Group D component some recent radiogenic Pb loss would need to be invoked, yet Group M, which is higher in U content, has less evidence of any Pb loss process. Hence, an alternative that Group D reflects peritectic growth with crystallizing liquid heterogeneity leading to some titanite genesis in U and REE starved domains, with greater proportion of common Pb, is also viable.

3.4.2. Sample 7441

The total heavy rare earth elements (HREE: from Ho to Lu) in the titanite from Bjørneøen sample 7441 are strongly depleted compared to the totals of LREE (La to Nd; Fig. 9). In addition, these titanite grains show conspicuous positive Eu anomalies (Eu/Eu*). Th/U ratios (mean = 0.5) are distinctly lower than in sample 308309 (mean = 12.9), compatible with an origin from a fluid involving both silicate and water-hydrothermal components, as opposed to growth from pure silicate melt. Such a fluid may originate from dehydration plus minor melting during prograde metamorphism. Additionally, the positive Eu/Eu* is consistent with a metamorphic genesis as Eu^{+2} is more soluble than other REE in hydrothermal fluids. Horie et al. (2008) reported similar positive Eu/Eu* in titanite from experimental products grown under reducing hydrothermal conditions. These authors suggested positive Eu anomalies result from incorporation of Eu^{2+} together with Ca^{2+} into the titanite.

The total REE content is on average lower for apparently younger titanite in this sample and we interpret this relationship to be a consequence of post crystallization diffusion or alteration associated with
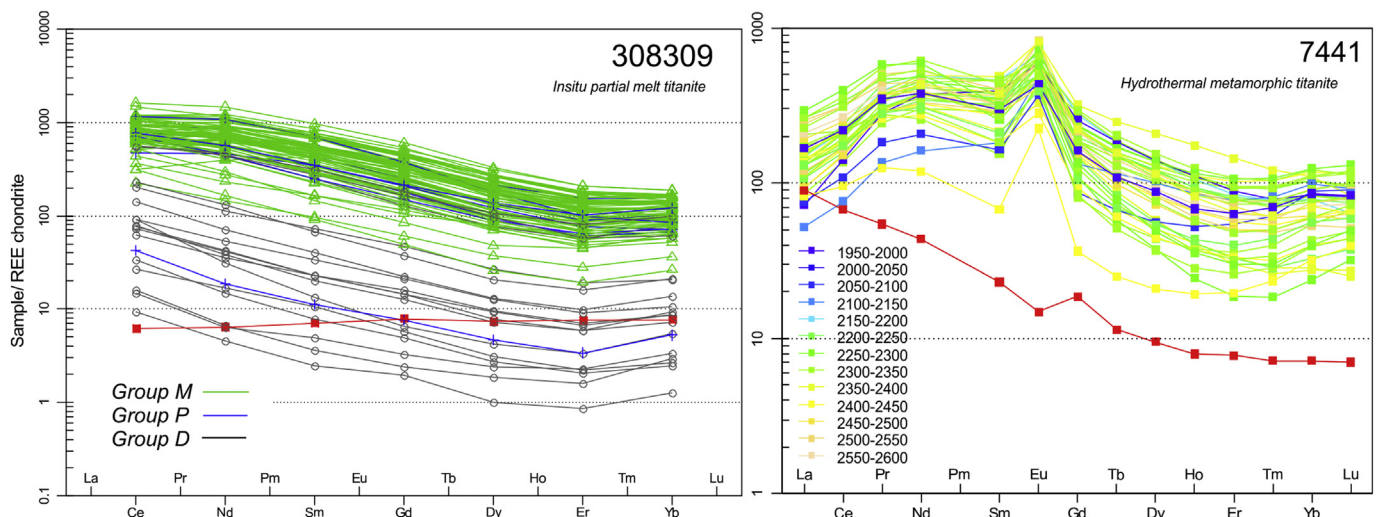
Fig. 9. Chondrite normalized REE plots of titanite from 308309 (left) and 7441 (right). Whole rock REE pattern denoted by red trace (note for 308309 this reflects the leucosome absent component). 308309 is coloured according to interpreted titanite groups. 7441 is colour scaled according to 207-corrected date (in Ma). (For interpretation of the references to colour in this figure legend, the reader is referred to the web version of this article.)

loss of radiogenic-Pb. Although the measured concentrations of Zr in titanite place the *P–T* conditions into the stability field of anatectic melt, a slightly drier (i.e. H_2O-poor) composition would move the solidus to higher temperatures, but the same mineral assemblage would be stable albeit at subsolidus conditions (e.g. White et al., 2005). Therefore, the estimated *P–T* conditions of titanite stability and the measured Zr-in-titanite concentrations are broadly compatible.

4. Discussion

4.1. Metamorphic conditions

4.1.1. Temperature estimates from titanite

In sample 308309, titanite growth at c. 2536 Ma is estimated to have occurred at < 750 °C based on phase equilibrium modelling (Fig. 7a). This temperature is compatible with the concentrations of Zr-in-titanite using the thermometer formulation of Hayden et al. (2008) and considering the activities of titania in a rutile-absent system (Fig. 7b), which given the absence of rutile in this sample is consistent with titania activities of < 1.0. The titanite growth is inferred to have been at lower pressure and temperature conditions than the 2857–2700 Ma ductile deformation event (820–850 °C and 8–10 kbar; Kirkland et al., 2018a), and are compatible with the modelled *P–T* field of < 700 °C at < 6 kbar where titanite is predicted to have concentrations of Zr similar to the measured values (Fig. 7e). Sample 308,309 Group M Zr-in titanite temperatures are greater than temperatures estimate from Groups D and P, which we interpret to reflect cryptic secondary alteration processes. Individual Group M Zr-in titanite temperatures spread to lower temperatures from a maximum of around 690 °C, which likely best represents the growth temperature of this titanite from a silicate-based melt (Fig. 10).

Titanite from sample 7441 is interpreted to reflect a single growth event that has been subject to later radiogenic-Pb mobility. Using a value of 0.7 for $aTiO_2$ (relative to rutile; Fig. 8), $aSiO_2$ held at unity and a pressure of 6 kbar, yields individual Zr-in titanite temperatures of 627 °C to 724 °C, with a weighted mean of 667 ± 6 °C (MSWD = 1.4; N = 38 of 39; Fig. 11). We interpret this average temperature to reflect a best estimate for the hydrothermal (+melt) event that grew these grains during fluid–rock interaction.
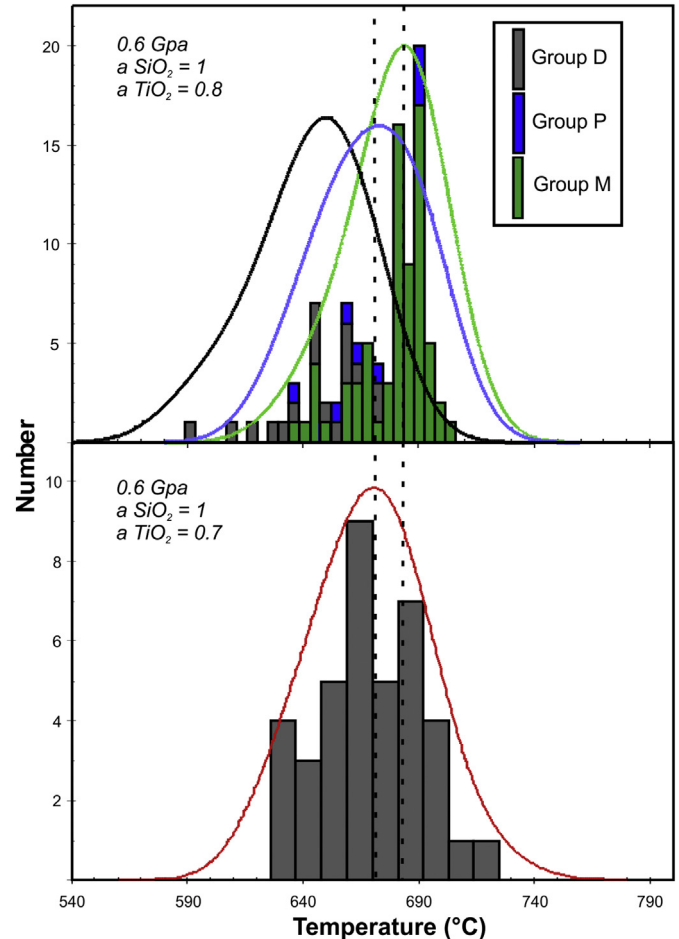

Fig. 10. Upper, Combined histogram and probability plot of Zr-in-titanite temperatures (°C) for the different titanite groups in sample 308309. The higher temperatures in this distribution are interpreted to more likely reflect formation temperatures due to post crystallization alternation in Groups P and D. Lower, Combined histogram and probability plot of Zr-in-titanite temperatures (°C) for titanite in sample 7441.
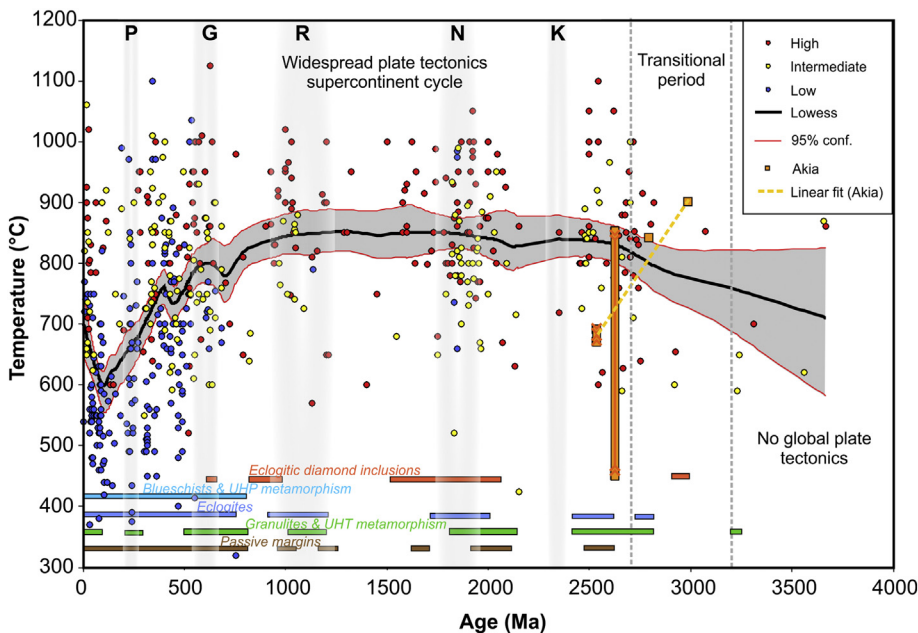
4.2. Thermal events in the Akia Terrane

The continental crust that today comprises the Akia Terrane formed during two episodes of magmatism: a dioritic component at c. 3.2 Ga (which dominated in the south) and a tonalitic component at c. 3.0 Ga (which dominated in the north) (Garde, 1997; Garde et al., 2000; Gardiner et al., 2019). The geodynamic setting of the 3.2 Ga event is cryptic. Preliminary Re−Os isotope data for highly forsteritic peridotites in Fiskefjord in the central Akia Terrane yield imply they were formed during this event (Szilas et al., 2016). These rocks likely reflect extremely high degrees of partial melting of their mantle source, possibly within a mantle plume setting (Szilas et al., 2018), with the implication that this may also be the setting for 3.2 Ga diorite. Alternatively, the diorites have been interpreted as forming within an island arc type setting (Garde, 1997; Garde et al., 2000).

The voluminous 3.0 Ga tonalitic crust was proposed by Garde (1997) to have also formed in a convergent (arc-related) plate tectonic setting, with meta-andesites in the Qussuk-Bjørneøen supracrustal sequence, part of the southern Akia Terrane, also interpreted to have formed by subduction zone processes at c. 3.0 Ga (Szilas et al., 2017). However, Gardiner et al. (2019) showed, on the basis of Hf isotopes in zircon, that the two main magmatic events of the Akia Terrane likely incorporated Eoarchean or older mafic crust (up to 800 Ma older), and that the tonalitic component has whole-rock trace-element patterns implying it was formed during deep melting in the presence of garnet. Gardiner et al. (2019) suggested that on these lines of evidence, and on the remarkable age and chemical homogeneity of the c. 3.0 Ga tonalitic crust, that the continental crust of the Akia Terrane may have had its genesis through protracted deep melting of old, thick mafic crust. These authors suggested this scenario may be hard to reconcile with an island arc model, and instead may have affinities with vertical tectonic-type geodynamic models, such as the East Pilbara Terrane of Western Australia, where mafic crust thickens through episodic volcanic overburden (Smithies et al., 2005) to reach a critical thickness where it infracrustally melts. Furthermore, the presence of undeformed two-pyroxene leucosomes in c. 3.0 Ga metamafic migmatites as well as the results of phase equilibrium and trace-element modelling led Yakymchuk et al., 2020 to argue that generation of tonalites in the Akia Terrane during high-temperature–low-pressure metamorphism was in a static environment that did not require subduction and arc magmatism.

Subsequent metamorphic mineral growth is recorded by widespread

U−Pb ages of metamorphic zircon between 2.85 and 2.75 Ga (Kirkland et al., 2018a). This wide age spread may imply a prolonged thermal event, or that some of the U−Pb dates may be affected by extreme temperatures driving Pb diffusion in zircon. In any case, the 2.85–2.75 Ga metamorphic event in the Akia Terrane is broadly coeval with events within the Kapisillit, Tre Brødre, and Tasiusaesuaq terranes to the south (Næraa and Scherstén, 2008; Nutman and Friend, 2007; Friend and Nutman, 1994). Such communal thermal history implies tectonic links across some 300 km of strike length. Modern orogenic-style accretion south of the Akia Terrane was likely responsible for a thermal event at c. 2.72 Ga, as evidenced by high-pressure metamorphism in a clock-wise P–T path (Nutman et al., 1989; Nutman and Friend, 2007; Dziggel et al., 2014). Both the 2.85–2.75 and 2.72 Ga metamorphic events were interpreted as the result of compressive tectonic regimes at an orogenic margin by Kolb et al. (2012), which would support the operation of local plate tectonic processes, probably linked to the assembly of the North Atlantic Craton at least since the Neoarchean in this region (e.g. Friend et al., 1988; McGregor et al., 1991; Friend et al., 1996).

Later minor magmatic events at c. 2.7 and 2.5 Ga are predominantly granitic (sensu stricto). Within the northern Akia Terrane these magmatic events have zircon εHf which lies on an evolution trend from the older 3.0 Ga tonalities and are therefore interpreted as the product of reworking of the existing tonalitic crust (Gardiner et al., 2019). The c. 2.7 Ga event, manifest as pegmatites and minor granite sheets, is likely the result of local anataxis during regional terrane shuffling due to further compression across the region (Friend et al., 1996), again linked to craton assembly. Effects of a 2.5 Ga tectonothermal event are widely visible in the outcropping geology of the region, for example the extensive c. 2.55 Ga Qôrqut Granite Complex in the Nuuk-region (McGregor, 1973; Brown et al., 1981; Nutman et al., 2010; Naeraa et al., 2014). This granite body has been proposed to have formed as a result of percolating meteoritic fluids into dilatational fractures promoting crustal melting (Nutman et al., 2010). A geodynamic setting involving widespread elevated crustal water flux throughout and within North Atlantic Craton terranes at c. 2.55 Ga is consistent with metamorphic titanite growth and localised in situ partial melting at this time in the Akia Terrane.

4.3. Implications for North Atlantic geodynamic state through time

We show the Akia Terrane experienced a distinct change in thermal style during the Meso-Neoarchean, from major crust-forming events up to 3.0 Ga, immediately followed by granulite-facies metamorphism, and then later magmatism and lower temperature metamorphism linked to terrane assembly and post-assembly tectonic movements. On the basis of titanite geochronology coupled with phase equilibrium modelling, Pb diffusion modelling, and mineral trace-element thermometry, we discern a cycle of mineral growth events coupled with thermal and fluid perturbation in the Akia Terrane at approximately every 100 Ma from c. 2.8 Ga (Fig. 11). Bédard and Harris (2014) and Bédard (2018) have suggested a similar (broadly 120 Ma) period between magmatic events in the Neoarchaean Superior Craton in Canada, which they ascribed to thermal incubation between mantle overturn events. However, a 100 Ma period is also recognised as the approximate lifetime of an ocean from creation to destruction in the horizontal plate regime which dominated Proterozoic Earth (Kirkland et al., 2017).

Brown and Johnson (2018) have discussed the thermal state of the Earth through time and linked secular changes in pressures and temperatures inferred from the metamorphic record to shifts in geodynamics. A comparison of the temperature time record of the Akia Terrane with the Brown and Johnson et al. (2018) global metamorphic temperature compilation is shown in Fig. 11. It is clear that mantle potential temperature was higher in the Archean (e.g., Herzberg, 2011). Prior to c. 3.0 Ga, heating from radioactive decay was expected to have exceeded surface heat loss, in contrast to conditions post 3.0 Ga when secular cooling has been proposed to have dominated the thermal state of the planet (Korenaga, 2008). Before 3.0 Ga, the crustal record of metamorphism is sparse, as evident in the compilation of Brown and Johnson (2018). Nonetheless, a LOWESS curve (Fig. 11; black line) fitted to all available crustal metamorphic temperatures rises to a broad plateau that commences from about 3.0 Ga, with a precipitous fall from average metamorphic temperatures of around 820 °C in the Cambrian where low T/P gradients are common (e.g. depressed isotherms at subduction zones; Fig. 11).

The Akia Terrane reveals a changing thermal structure, where early metamorphism at 3.0 Ga was associated with granulite-facies conditions at potentially some of the highest temperature conditions recorded for that time period globally (Yakymchuk et al., 2020), whereas by c. 2.54 Ga metamorphic temperatures had significantly decreased and were associated with a widespread water-fluxed hydrothermal environment linked to orogenic processes driving craton assembly (McGregor and Friend, 1992; Friend et al., 1996; Naeraa et al., 2014; Gardiner et al., 2020).

5. Conclusions

Two titanite samples in the Akia Terrane both yield a U−Pb age of c. 2540 Ma. Although apparently coeval, these two samples formed under distinctly different processes. In one case, titanite grew from a silicate in-situ partial melt, consistent with its distinct geochemistry (elevated total REE and high Th/U ratios). In contrast, titanite elsewhere in the Akia Terrane grew within a system dominated by hydrothermal solutions and contains greater common Pb, lower Th/U, lower total REE, and was more susceptible to later radiogenic Pb mobility. These results illustrate that variable mineral growth process can be coeval, related to the same larger thermal/fluid anomaly.

Phase equilibrium modelling was used to quantify the activity of titania in rutile-absent systems and refine temperature estimates from the Zr in titanite thermometer; using a titania activity of 0.7 instead of 1.0 reduces the calculated temperature by ~20 °C.

New geochronology coupled with mineral chemistry and phase equilibrium modelling in combination with existing published data reveals punctuated, repeated magmatism and metamorphism in the Akia Terrane, in which high temperature conditions reoccurred at least

three times between 3.0 and 2.5 Ga. Analysis of magmatic titanite from the Akia Terrane yields a maximum Zr-in-titanite temperature of c. 690 °C at c. 2536 Ma, coeval with crystallization of regional granitic magmas. In contrast, hydrothermal titanite indicates conditions of c. 670 °C at approximately the same time.

We show that meaningful U−Pb ages can be recovered from titanite with high common Pb contents, via petrographic identification and subsequent measurement of a coeval U free but Pb rich mineral (e.g. biotite) that pins initial $^{207}Pb/^{206}Pb$. When this temporal information is allied with phase equilibria modelling and trace-element chemistry, titanite provides a powerful means to trace time temperature pathways and fluid rock interaction, ultimately helping to resolve crustal geodynamic state.

Supplementary data to this article can be found online at https://doi.org/10.1016/j.chemgeo.2020.119467.

References

Aleinikoff, J.N., Wintsch, R.P., Tollo, R.P., Unruh, D.M., Fanning, C.M., Schmitz, M.D., 2007. Ages and origins of rocks of the Killingworth dome, south-central Connecticut: Implications for the tectonic evolution of southern New England. Am. J. Sci. 307 (1), 63–118.

Baadsgaard, H., McGregor, V.R., 1981. The U-Th-Pb systematics of zircons from the type Nûk gneisses, Godthåbsfjord, west Greenland. Geochim. Cosmochim. Acta 50, 2173–2183.

Bédard, J.H., 2018. Stagnant lids and mantle overturns: Implications for Archaean tectonics, magmagenesis, crustal growth, mantle evolution, and the start of plate tectonics. Geosci. Front. 9 (2018), 19–49.

Bédard, J.H., Harris, L.B., 2014. Neoarchean disaggregation and reassembly of the Superior craton. Geology 42, 951–954.

Bridgwater, D., McGregor, V.R., Myers, J.S., 1974. A horizontal tectonic regime in the Archaean of Greenland and its implications for early crustal thickening. Precambrian Res. 1 (3), 179–197.

Brown, M., Johnson, T., 2018. Secular change in metamorphism and the onset of global plate tectonics. Am. Mineral. 103, 181–196.

Brown, M., Friend, C.R.L., McGregor, V.R., Perkins, W.T., 1981. The Late Archaean Qôrqut granite complex of southern west Greenland. J. Geophys. Res. 86 (B11), 10617–10632.

Cawood, P.A., Hawkesworth, C.J., Pisarevsky, S.A., Dhuime, B., Capitanio, F.A., Nebel, O., 2018. Geological archive of the onset of plate tectonics. Phil. Trans. R. Soc. A 376, 20170405.

Cherniak, D.J., 1995. Sr and Nd diffusion in titanite. Chem. Geol. 125 (3–4), 219–232.

Chew, D., Petrus, J., Kamber, B., 2014. U–Pb LA–ICPMS dating using accessory mineral standards with variable common Pb. Chem. Geol. 363, 185–199.

Corfu, F., 1996. Multistage zircon and titanite growth and inheritance in an Archean gneiss complex, Winnipeg River subprovince, Ontario. Earth Planet. Sci. Lett. 141 (1–4), 175–186.

Dhuime, B., Hawkesworth, C.J., Cawood, P.A., Storey, C.D., 2012. A change in the geodynamics of continental growth 3 billion years ago. Science 335, 1334–1336.

Dziggel, A., Diener, J.F.A., Kolb, J., Kokfelt, T.F., 2014. Metamorphic record of accretionary processes during the Neoarchaean: the Nuuk region, southern west Greenland. Precambrian Res. 242, 22–38.

Friend, C.R.L., Nutman, A.P., 1994. Two Archaean granulite-facies metamorphic events in the Nuuk-Maniitsoq region, southern west Greenland: correlation with the Saglek block, Labrador. J. Geol. Soc. Lond. 151, 421–424.

Friend, C.R.L., Nutman, A.P., 2005. New pieces to the Archaean terrane jigsaw puzzle in the Nuuk region, southern west Greenland: steps in transforming a simple insight into a complex regional tectonothermal model. J. Geol. Soc. 162 (1), 147–162.

Friend, C.R.L., Nutman, A.P., 2019. Tectono-stratigraphic terranes in Archaean gneiss complexes as evidence for plate tectonics: the Nuuk region, southern west Greenland. Gondwana Res. 72, 213–237.

Friend, C.R.L., Nutman, A.P., McGregor, V.R., 1988. Late Archaean terrane accretion in the Godthåb region, southern west Greenland. Nature 335, 535–538.

Friend, C.R.L., Nutman, A.P., Baadsgaard, H., Kinny, P.D., McGregor, V.R., 1996. Timing of late Archaean terrane assembly, crustal thickening and granite emplacement in the Nuuk region, southern west Greenland. Earth Planet. Sci. Lett. 142 (3–4), 353–365.

Gao, X.-Y., Zheng, Y.-F., Chen, Y.-X., Guo, J., 2012. Geochemical and U–Pb age constraints on the occurrence of polygenetic titanites in UHP metagranite in the Dabie orogen. Lithos 136, 93–108.

Garber, J., Hacker, B., Kylander-Clark, A., Stearns, M., Seward, G., 2017. Controls on trace element uptake in metamorphic titanite: implications for petrochronology. J. Petrol. 58 (6), 1031–1057.

Garde, A.A., 1997. Accretion and evolution of an Archaean high-grade grey gneiss-amphibolite complex: the Fiskefjord area, southern west Greenland. Geol. Greenl. Surv. Bull. 17.

Garde, A.A., 2007. A mid-Archaean island arc complex in the eastern Akia terrane, Godthåbsfjord, southern west Greenland. J. Geol. Soc. 164 (3), 565–579.

Garde, A.A., Friend, C., Nutman, A., Marker, M., 2000. Rapid maturation and stabilisation of middle Archaean continental crust: the Akia terrane, southern west Greenland. Bull. Geol. Soc. Den. 47, 1–27.

Garde, A.A., McDonald, I., Dyck, B., Keulen, N., 2012. Searching for giant, ancient impact structures on Earth: the Mesoarchaean Maniitsoq structure, west Greenland. Earth Planet. Sci. Lett. 337–338, 197–210.

Garde, A.A., Dyck, B., Esbensen, K.H., Johansson, L., Möller, C., 2014. The Finnefjeld domain, Maniitsoq structure, west Greenland: differential rheological features and mechanical homogenisation in response to impacting? Precambrian Res. 255, 791–808.

Gardiner, N.J., Kirkland, C.L., Van Kranendonk, M.J., 2016. The Juvenile Hafnium isotope signal as a record of supercontinent cycles. Sci. Rep. 6, 38503.

Gardiner, N.J., Kirkland, C.L., Hollis, J., Cawood, P., Nebel, O., Szilas, K., Yakymchuk, C., 2020. North Atlantic Craton Architecture revealed by kimberlite-hosted crustal zircons. EPSL In press.

Gardiner, N.J., Kirkland, C.K., Hollis, J., Szilas, K., Steenfelt, A., Yakymchuk, C., Heide-Jørgensen, H., 2019. Building Mesoarchaean crust upon Eoarchaean roots: the Akia Terrane, west Greenland. Contrib. Mineral. Petrol. 174 (20), 1–19.

Ghiorso, M.S., Gualda, G.A.R., 2013. A method for estimating the activity of titania in magmatic liquids from the compositions of coexisting rhombohedral and cubic iron-titanium oxides. Contrib. Mineral. Petrol. 165, 73–81.

Green, E.C.R., White, R.W., Diener, J.F.A., Powell, R., Holland, T.J.B., Palin, R.M., 2016. Activity–composition relations for the calculation of partial melting equilibria in metabasic rocks. J. Metamorph. Geol. 34, 845–869.

Hartnady, M.I.H., Kirkland, C.L., 2019. A gradual transition to plate tectonics on Earth between 3.2 and 2.7 billion years ago. Terra Nova 31, 129–134.

Hartnady, M.I.H., Kirkland, C.L., Clark, C., Spaggiari, C.V., Smithies, R.H., Evans, N.J., McDonald, B.J., 2019. Titanite dates crystallisation; slow Pb diffusion during supersolidus re-equilibration. J. Metamorph. Geol. 37, 823–838.

Hayden, L.A., Watson, E.B., Wark, D.A., 2008. A thermobarometer for sphene (titanite). Contrib. Mineral. Petrol. 155 (4), 529–540.

Henderson, P., 1980. Rare earth element partition between sphene, apatite and other coexisting minerals of the Kangerdlugssuaq intrusion, E. Greenland. Contrib. Mineral. Petrol. 72, 81–85.

Herzberg, C., 2011. Basalts as temperature probes of earth's mantle. Geology 39 (12), 1179–1180.

Holland, T.J.B., Powell, R., 2011. An improved and extended internally consistent thermodynamic dataset for phases of petrological interest, involving a new equation of state for solids. J. Metamorph. Geol. 29, 333–383.

Horie, K., Hidaka, H., Gauthier-Lafaye, F., 2008. Elemental distribution in apatite, titanite and zircon during hydrothermal alteration: durability of immobilization mineral phases for actinides. Phys. Chem. Earth A/B/C 33 (14–16), 962–968.

Horn, I., von Blanckenburg, F., 2007. Investigation on elemental and isotopic fractionation during 196 nm femtosecond laser ablation multiple collector inductively coupled plasma mass spectrometry. Spectrochim. Acta B At. Spectrosc. 62 (4), 410–422.

Johnson, T.E., Brown, M., Gardiner, N.J., Kirkland, C.L., Smithies, R.H., 2017. Earth's first stable continents did not form by subduction. Nature 543, 239–242.

Johnson, T.E., Gardiner, N.J., Miljkovic, K., Spencer, C.J., Kirkland, C.L., Bland, P.A., Smithes, R.H., 2018. An impact melt origin for earth's oldest known evolved rocks. Nat. Geosci. 11, 795–799.

Kennedy, A.K., Kamo, S.L., Nasdala, L., Timms, N.E., 2010. Grenville skarn titanite: potential reference material for SIMS U–Th–Pb analysis. Can. Mineral. 48 (6), 1423–1443.

Keulen, N., Garde, A.A., Jørgart, T., 2015. Shock melting of K-feldspar and interlacing with cataclastically deformed plagioclase in granitic rocks at Toqqusap Nunaa, southern west Greenland: implications for the genesis of the Maniitsoq structure. Tectonophysics 662, 328–344.

Kirkland, C.L., Daly, J.S., Whitehouse, M.J., 2008. Basement–cover Relationships of the Kalak Nappe Complex, Arctic Norwegian Caledonides and Constraints on Neoproterozoic Terrane Assembly in the North Atlantic Region. 160. pp. 245–276.

Kirkland, C.L., Smithies, R., Spaggiari, C., Wingate, M., Quentin de Gromard, R., Clark, C., Gardiner, N., 2017. Proterozoic crustal evolution of the Eucla basement, Australia: implications for destruction of oceanic crust during emergence of Nuna. Lithos 278–281, 427–444.

Kirkland, C.L., Yakymchuk, C., Hollis, J., Heide-Jørgensen, H., Danišík, M., 2018a. Mesoarchean exhumation of the Akia terrane and a common Neoarchean tectonothermal history for west Greenland. Precambrian Res. 314, 129–144.

Kirkland, C.L., Yakymchuk, C., Szilas, K., Evans, N., Hollis, J., McDonald, B., Gardiner, N.J., 2018b. Apatite: a U-Pb thermochronometer or geochronometer? Lithos 318-319, 143–157.

Kirkland, C.L., Fougerouse, D., Reddy, S.M., Hollis, J., Saxey, D.W., 2018c. Assessing the mechanisms of common Pb incorporation into titanite. Chem. Geol. 483, 558–566.

Kohn, M.J., 2017. Titanite petrochronology. Rev. Mineral. Geochem. 83 (1), 419–441.

Kohn, M.J., Corrie, S.L., 2011. Preserved Zr-temperatures and U-Pb ages in high-grade metamorphic titanite: evidence for a static hot channel in the Himalayan orogen. Earth Planet. Sci. Lett. 311 (1–2), 136–143.

Kolb, J., Kokfelt, T.F., Dziggel, A., 2012. Geodynamic setting and deformation history of an Archaean terrane at mid-crustal level: the Tasiusarsuaq terrane of southern west Greenland. Precambrian Res. 212, 34–56.

Korenaga, J., 2008. Urey ratio and the structure and evolution of Earth's mantle. Rev. Geophys. 46, RG2007.

Kusky, T.M., Windley, B.F., Polat, A., 2018. Geological evidence for the operation of Plate Tectonics throughout the Archean: Records from Archean Paleo-Plate Boundaries. J. Earth Sci. 29 (6), 1291–1303.

Kylander-Clark, A., Hacker, B., Mattinson, J., 2008. Slow exhumation of UHP terranes: titanite and rutile ages of the Western Gneiss Region, Norway. Earth Planet. Sci. Lett. 272 (3–4), 531–540.

Latypov, R., Chistyakova, S., Grieve, R., Huhma, H., 2019. Evidence for igneous differentiation in Sudbury Igneous complex and impact-driven evolution of terrestrial planet proto-crusts. Nat. Commun. 10, 508.

McFarlane, C.R.M., 2016. Allanite U/Pb geochronology by 193 nm LA ICP-MS using NIST610 glass for external calibration. Chem. Geol. 438, 91–102.

McGregor, V.R., 1973. The early Precambrian gneisses of the Godthåb district. West Greenland Phil. Trans. Royal Soc. London A273, 343–358.

McGregor, V.R., Friend, C.R.L., 1992. Late Archean prograde amphibolite- to granulite-facies relations in the Fiskenæsset region, southern west Greenland. J. Geol. 100, 207–219.

McGregor, V.R., Friend, C.R.L., Nutman, A.P., 1991. The late Archaean mobile belt through Godthåbsfjord, southern west Greenland: a continent-continent collision zone? Geological Society of Denmark Bulletin 39, 179–197.

Næraa, T., Scherstén, A., 2008. New zircon ages from the Tasiusarsuaq terrane, southern west Greenland. Geological Survey of Denmark and Greenland Bulletin 15, 73–76.

Naeraa, T., Scherstén, A., Rosing, M.T., Kemp, A.I.S., Hoffmann, J.E., Kokfelt, T.F., Whitehouse, M.J., 2012. Hafnium isotope evidence for a transition in the dynamics of continental growth 3.2 Gyr ago. Nature 485 (7400), 627.

Naeraa, T., Kemp, A.I.S., Scherstén, A., Rehnstrom, E.F., Rosing, M.T., Whitehouse, M.J., 2014. A lower crustal mafic source for the ca. 2550 Ma Qorqut granite complex in southern west Greenland. Lithos 192, 291–304.

Nutman, A.P., Friend, C.R.L., 2007. Adjacent terranes with ca.2715 and 2650 Ma high-pressure metamorphic assemblages in the Nuuk region of the North Atlantic Craton, southern west Greenland: complexities of Neoarchaean collisional orogeny. Precambrian Res. 155 (3–4), 159–203.

Nutman, A.P., Friend, C.R.L., Baadsgaard, H., McGregor, V.R., 1989. Evolution and assembly of Archaean gneiss terranes in the Godthåbsfjord region, southern west Greenland: structural, metamorphic, and isotopic evidence. Tectonics 8, 573–589.

Nutman, A.P., Christiansen, O., Friend, C.R., 2007. 2635 Ma amphibolite facies gold mineralisation near a terrane boundary (suture?) on Storø, Nuuk region, southern west Greenland. Precambrian Res. 159 (1–2), 19–32.

Nutman, A.P., Friend, C.R., Hiess, J., 2010. Setting of the ~2560 Ma Qôrqut Granite complex in the Archean crustal evolution of southern west Greenland. Am. J. Sci. 310 (9), 1081–1114.

Olierook, H.K.H., Taylor, R.J.M., Erickson, T.M., Clark, C., Reddy, S.M., Kirkland, C.L., Jahn, I., Barham, M., 2019. Unravelling complex geologic histories using U–Pb and trace element systematics of titanite. Chem. Geol. 504, 105–122.

Palin, R.M., White, R.W., Green, E.C., Diener, J.F., Powell, R., Holland, T.J., 2016. High-grade metamorphism and partial melting of basic and intermediate rocks. J. Metamorph. Geol. 34, 871–892. https://doi.org/10.1111/jmg.12212.

Paton, C., Woodhead, J.D., Hellstrom, J.C., Hergt, J.M., Greig, A., Maas, R., 2010. Improved laser ablation U-Pb zircon geochronology through robust downhole fractionation correction. Geochem. Geophys. Geosyst. 11 (3).

Paton, C., Hellstrom, J., Paul, B., Woodhead, J., Hergt, J., 2011. Iolite: freeware for the visualisation and processing of mass spectrometric data. J. Anal. At. Spectrom. 26 (12), 2508–2518.

Powell, R., Holland, T.J.B., 1988. An internally consistent dataset with uncertainties and correlations: 3. Applications to geobarometry, worked examples and a computer program. J. Metamorph. Geol. 6, 173–204.

Prowatke, S., Klemme, S., 2005. Effect of melt composition on the partitioning of trace elements between titanite and silicate melt. Geochim. Cosmochim. Acta 69 (3), 695–709.

Riciputi, L.R., Valley, J.W., McGregor, V.R., 1990. Conditions of Archean granulite metamorphism in the Godthab-Fiskenaesset region, southern west Greenland. J. Metamorph. Geol. 8, 171–190.

Scherstén, A., Garde, A.A., 2013. Complete hydrothermal re-equilibration of zircon in the Maniitsoq structure, west Greenland: a 3001 Ma minimum age of impact? Meteorit. Planet. Sci. 48, 1472–1498.

Shirey, S.B., Richardson, S.H., 2011. Start of the Wilson cycle at 3 Ga shown by diamonds from subcontinental mantle. Science 333, 434–436.

Sláma, J., Kosler, J., Condon, D.J., Crowley, J.L., Gerdes, A., Hanchar, J.M., Horstwood, M.S.A., Morris, G.A., Nasdala, L., Norberg, N., Schaltegger, U., Schoene, B., Tubrett, M.N., Whitehouse, M.J., 2008. Plesovice zircon - a new natural reference material for

U-Pb and Hf isotopic microanalysis. Chemical Geology 249 (1-2), 1–35.

Smith, M.P., Storey, C.D., Jeffries, T.E., Ryan, C., 2009. In situ U–Pb and trace element analysis of accessory minerals in the Kiruna district, Norrbotten, Sweden: new constraints on the timing and origin of mineralization. J. Petrol. 50 (11), 2063–2094.

Smithies, R.H., Champion, D.C., Van Kranendonk, M.J., Howard, H.M., Hickman, A.H., 2005. Modern-style subduction processes in the Mesoarchaean: geochemical evidence from the 3.12 Ga Whundo intraoceanic arc. Earth Planet. Sci. Lett. 231, 221–237.

Smithies, R.H., Van Kranendonk, M.J., Champion, D.C., 2007. The Mesoarchean emergence of modern-style subduction. Gondwana Res. 11 (1/2), 50–68.

Spandler, C., Hammerli, J., Sha, P., Hilbert-Wolf, H., Hu, Y., Roberts, E., et al., 2016. MKED1: a new titanite standard for in situ analysis of Sm–Nd isotopes and U–Pb geochronology. Chem. Geol. 425, 110–126.

Stacey, J.T., Kramers, J., 1975. Approximation of terrestrial lead isotope evolution by a two-stage model. Earth Planet. Sci. Lett. 26 (2), 207–221.

Storey, C.D., Smith, M.P., Jeffries, T.E., 2007. In situ LA-ICP-MS U-Pb dating of metavolcanics of Norrbotten, Sweden: records of extended geological histories in complex titanite grains. Chem. Geol. 240, 163–181.

Szilas, K., van Hinsberg, V.J., McDonald, I., Morishita, T., Pearson, D.G., 2016. Highly Depleted Peridotites Within Mesoarchaean Orthogneiss at the Seqi Olivine Mine, SW Greenland e Potential Implications for the Formation of Cratonic Keels. Goldschmidt Conference, Abstract 3009, Yokohama.

Szilas, K., Tusch, J., Hoffmann, J.E., Garde, A.A., Münker, C., 2017. Hafnium isotope constraints on the origin of Mesoarchaean andesites in southern west Greenland, North Atlantic craton. Geol. Soc. Lond., Spec. Publ. 449 (1), 19–38.

Szilas, K., van Hinsberg, V., McDonald, I., Næraa, T., Rollinson, H., Adetunji, J., Bird, D., 2018. Highly refractory Archaean peridotite cumulates: petrology and geochemistry of the Seqi Ultramafic complex, SW Greenland. Geosci. Front. 9 (3), 689–714.

Talbot, C.J., 1973. A plate tectonic model for the Archaean crust. Phil. Trans. R. Soc. London A273, 413–427.

Tiepolo, M., Oberti, R., Vannucci, R., 2002. Trace-element incorporation in titanite: constraints from experimentally determined solid/liquid partition coefficients. Chem. Geol. 191 (1–3), 105–119.

Walters, J.B., Kohn, M.J., 2017. Protracted thrusting followed by late rapid cooling of the Greater Himalayan sequence, Annapurna Himalaya, central Nepal: insights from titanite petrochronology. J. Metamorph. Geol. 35 (8), 897–917.

White, R.W., Pomroy, N.E., Powell, R., 2005. An in situ metatexite–diatexite transition in upper amphibolite facies rocks from Broken Hill, Australia. J. Metamorph. Geol. 23, 579–602.

Yakymchuk, C., Kirkland, C.L., Hollis, J.A., Kendrick, J., Gardiner, N., Szilas, K., 2019. Reworking of Mesoarchean crust during high-temperature–low-pressure metamorphism, Akia terrane, west Greenland. Precambrian Res in review.